Electronic Supporting Information for

Redox Properties and Electron Transfer in a Triarylamine-substituted HS-Co^{2+}/LS-Co^{3+} Redox Couple

Linda Schnaubelt[a)], Holm Petzold*[a)], J. Matthäus Speck[a)], Evgenia Dmitrieva[b)], Marco Rosenkranz[b),] Marcus Korb[a)]

a) TU Chemnitz, Institut für Chemie, Anorganische Chemie, Straße der Nationen 62, 09111 Chemnitz, Germany; Fax: +49-371-53137463; E-mail: holm.petzold@chemie.tu-chemnitz.de

b) Center of Spectroelectrochemistry, Leibniz Institute for Solid State and Materials Research (IFW Dresden), Helmholtzstrasse 20, 01069 Dresden, Germany

1. Supporting information

Table of content

1.1 Synthesis – general remarks

All reactions handling sensitive chemicals were carried out under argon using standard Schlenk and cannula techniques. THF was purified by distillation from sodium/benzophenone ketyl. Dry ethanol was purchased commercially from Acros Organics. Dichloromethane was taken from a solvent purification system SPS-800 by MBraun. 2-(Pyridin-2-yl)-1,10-phenanthroline[1] and 4-(di-*p*-tolylamino)phenol[2] were prepared as reported in the literature. All other chemicals were purchased from commercial suppliers and were used without further purification.

NMR spectra were recorded with a Bruker Avance III 500 spectrometer; chemical shifts for ^{1}H and ^{13}C NMR are referenced internally to the residual protons and to the ^{13}C NMR signal of the deuterated solvent. Elemental analyses were performed using a Thermo FlashAE 1112 analyzer. Mass spectra were recorded with a Bruker micrOTOF-QIIa mass spectrometer operating in ESI mode (ESI = electrospray ionisation).

1.2 Synthesis of ligands

1.2.1 Synthesis of 2-(6-bromopyridin-2-yl)-1,10-phenanthroline (4)

2,6-Dibromopyridine (20 g, 86 mmol) was dissolved in 200 ml of dry THF, cooled to -80°C and ^{n}BuLi (92 mmol, 37 mL, 2.5 M in hexane) was added. After 20 min stirring at -80°C 1,10-phenanthroline (18 g, 100 mmol) dissolved in 200 ml of dry THF was added within a few minutes at -80°C. The reaction mixture was stirred for further 2 h at -80°C. After the addition of water (30 mL) the suspension was allowed to warm to ambient temperature. The solvents were reduced to about 100 mL and were extracted with CH_2Cl_2 (3x150 mL). To the combined organic phases activated MnO_2 (50 g) was added. The oxidation requires some hours and the progress can be monitored by NMR spectroscopy. After completed oxidation the solids were first washed with CH_2Cl_2 (40 mL) and then repeatedly extracted with CH_2Cl_2 (several 150 mL portions). Filtration over celite and reduction of the solvents to dryness yield the title compound as white solid (15 g, 44 mmol, 52 % based on 1,10-phenanthroline). The compound was identified by ^{1}H NMR spectroscopy based on data reported by R. P. Thummel et al.[3]

^{1}H NMR (500 MHz, $CDCl_3$, 300 K): 9.25 (d, *J* = 3.4 Hz, 1H), 8.99 (d, *J* = 7.6 Hz, 1H), 8.81 (d, *J* = 7.9 Hz, 1H), 8.38 (d, *J* = 8.1 Hz, 1H), 8.28 (d, *J* = 7.5 Hz, 1H), 7.84 (m, 2H), 7.77 (t, *J* = 7.7 Hz, 1H), 7.67 (dd, *J* = 7.9, 4.2 Hz, 1H), 7.55 ppm (d, *J* = 7.7 Hz, 1H). **^{13}C NMR** (125.80 MHz, $CDCl_3$, 300 K): 171.18, 157.27, 154.59, 150.26, 146.14, 145.54, 141.34, 139.39, 137.05, 136.40, 129.10, 128.44, 127.04, 126.57, 123.08, 121.57, 121.05 ppm. **MS-ESI:** 336.0118 ([M+H]$^{+}$, calcd. 336.0136); 357.9940 ([M+Na]$^{+}$, calcd. 357.9956).

1.2.2 Synthesis of 4-((6-(1,10-phenanthrolin-2-yl)pyridin-2-yl)oxy)-*N*,*N*-di-*p*-tolylaniline (1)

Method 1: 500 mg (1.48 mmol) 2-(6-bromopyridin-2-yl)-1,10-phenanthroline (500 mg, 1.48 mmol), 4-(di-*p*-tolylamino)phenol (160 mg, 1.48 mmol)) and potassium *tert*-butoxide (166 mg, 1.48 mmol) were suspended in DMSO (8 mL) and heated to 135°C overnight. After cooling distilled water (15 mL) was added and the precipitate was separated using a centrifuge. The precipitates were washed with water twice, centrifuged again and extracted in CH_2Cl_2. The organic extracts were dried over $MgSO_4$, filtered and reduced to dryness using a rotary evaporator. To the remaining oil was added MeCN leading to a yellow solid. Drying in vacuum yield 361 mg of the title compound (45 % based on 2-(6-bromopyridin-2-yl)-1,10-phenanthroline).

EA calcd. for $C_{37}H_{28}NO \cdot H_2O \cdot$ ½ DMSO (%) C: 75.85, H: 5.53, N: 9.31; found C: 75.98, H: 5.11, N: 9.37. **^{1}H NMR** (500 MHz, $CDCl_3$, 300 K): 9.25 (dd, *J* = 4.3, 1.7 Hz, 1H, *H*1), 8.75 (dd, *J* = 7.5, 0.6 Hz, 1H, *H*8), 8.61 (d, *J* = 8.4 Hz, 1H, *H*6), 8.31 (d, *J* = 8.4 Hz, 1H, *H*7), 8.27 (dd, *J* = 8.1, 1.7 Hz, 1H, *H*3), 7.89 (t, *J* = 7.8 Hz, 1H, *H*9), 7.84 (d, *J* = 8.8 Hz, 1H, *H*5), 7.80 (d, *J* = 8.8 Hz, 1H, *H*4), 7.65 (dd, *J* = 8.0, 4.3 Hz, 1H, *H*2), 7.13 (d, *J* = 1.4 Hz, 4H, *H*11, *H*12), 7.09 (d, *J* = 8.3 Hz, 4H, *H*13/14), 7.04 (d, *J* = 8.5 Hz, 4H, *H*13/14), 6.94 (dd, *J* = 8.1, 0.7 Hz, 1H, *H*10), 2.32 ppm (s, 6H, *H*15). **^{13}C NMR** (125.80 MHz, $CDCl_3$, 300 K): 163.50, 155.86, 154.34, 150.55, 149.15, 146.51, 145.78, 145.75, 145.03, 140.52, 137.01, 136.36, 132.28, 130.00, 129.19, 128.98, 126.88, 126.73, 124.69, 124.19, 123.07, 122.14, 121.13, 117.35, 111.54, 20.93 ppm. **MS-ESI**: 545.2336 ([M+H]$^{+}$, calcd. 545.2336); 567.2155 ([M+Na]$^{+}$, calcd. 567.2150).

Method 2: 590 mg (2.04 mmol) 4-(di-*p*-tolylamino)phenol and 191 mg (1.70 mmol) potassium *tert*-butoxide were suspended in 3 mL of dry THF and heated to 60°C for 2 hours. After removing the solvent in vacuum 500 mg (1.48 mmol) of 2-(6-bromopyridin-2-yl)-1,10-phenanthroline was added and heated to 200°C for 4 hours. The chilled reaction mixture was dissolved in CH_2Cl_2, extracted with aqueous $NaHCO_3$ solution and dried over Na_2SO_4. All volatiles were removed under reduced pressure. Drying in vacuum yield 558 mg of the title compound (50 % based on 2-(6-bromopyridin-2-yl)-1,10-phenanthroline). The received compound was used without further purification.

1.2.3 Synthesis of 2-(6-phenoxypyridin-2-yl)-1,10-phenanthroline (2)

2-(6-bromopyridin-2-yl)-1,10-phenanthroline (500 mg, 1.48 mmol), phenol (139 mg, 1.48 mmol) and potassium *tert*-butoxide (166 mg, 1.48 mmol) were suspended in 8 mL of DMSO. The reaction mixture was heated to 135°C overnight. After cooling the reaction mixture was mixed with distilled water and centrifuged. The residue was washed with water and centrifuged twice. The solid was dissolved in CH_2Cl_2 and treated with *n*-hexane. The precipitate was removed and the solvent evaporated in oil pump vacuum to yield 517 mg of a yellow solid (73 % based on 2-(6-bromopyridin-2-yl)-1,10-phenanthroline).

EA calcd. for $C_{23}H_{15}N_3O \cdot ¼$ DMSO (%) C: 76.51, H: 4.51, N: 11.39; found C: 76.67, H: 4.47, N: 11.36. **^{1}H NMR** (500 MHz, $CDCl_3$, 300 K): 9.23 (dd, *J* = 4.4, 1.7 Hz, 1H, *H*1), 8.77 (dd, *J* = 7.5, 0.7 Hz, 1H, *H*8), 8.55 (d, *J* = 8.4 Hz, 1H, *H*6), 8.27 (dd, *J* = 8.2, 1.9 Hz, 2H, *H*7, *H*3), 7.87 (dd, *J* = 8.1, 7.6 Hz, 1H, *H*9), 7.81 (d, *J* = 8.8 Hz, 1H, *H*5), 7.78 (d, *J* = 8.8 Hz, 1H, *H*4), 7.65 (dd, *J* = 8.0, 4.4 Hz, 1H, *H*2), 7.47 – 7.42 (m, 2H, *H*11), 7.29 – 7.24 (m, 3H, *H*12, *H*13), 6.94 ppm (dd, *J* = 8.1, 0.7 Hz, 1H, *H*10). **^{13}C NMR** (125.80 MHz, $CDCl_3$, 300 K): 175.22, 163.02, 155.76, 154.44, 154.27, 150.05, 145.91, 145.29, 140.42, 136.89, 136.73, 129.58, 128.88, 126.74, 126.59, 124.48, 123.08, 121.22, 117.51, 111.81 ppm. **MS-ESI:** 350.1271 ($[M+H]^+$, calcd. 350.1288), 372.1098 ($[M+Na]^+$, calcd. 372.1107).

1.3 Synthesis of complexes

The ligand (1 eq) and the appropriate metal salt (1 eq) were suspended in 4 mL of dry EtOH and stirred overnight at ambient temperature. In this time the complexes precipitate from the solution. The precipitate was separated by centrifugation and washed with EtOH twice. The solid was dissolved in MeCN and filtered over Celite. The filtrate was mixed with Et_2O until precipitation formed and centrifuged. The solid was washed with Et_2O twice and dried in oil pump vacuum.

1.3.1 Synthesis of $[Co(1)_2](ClO_4)_2$

According to the general procedure 450 mg (0.83 mmol) of **1** and 303 mg (0.83 mmol) cobalt(II) perchlorate hexahydrate yield 361 mg (65 % based on **1**). In contrast to the single crystals used for structure analysis this material was dried in oil pump vacuum. The crystals weather by losing the packing solvents. To compensate the solvent loss, the voids refill with moisture water to saturate the ClO_4^- ions with hydrogen bonds. This is reflected in the elemental analysis.

EA calcd. for $C_{74}H_{56}Cl_2CoN_8O_{10} \cdot 2\ H_2O$ (%) C: 64.26, H: 4.37, N: 8.10; found C: 64.24, H: 4.15, N: 7.86. **^{1}H NMR** (500 MHz, d_3-MeCN, 300 K): 170.76 (bs, *LW* = 233 Hz, T_1 = 1.4 ms, 2H, *H*1), 113.86 (bs, *LW* = 56.7 Hz, T_1 = 12 ms, 2H, *H*7), 88.00 (bs, *LW* = 41.4 Hz, T_1 = 15 ms, 2H, *H*8), 45.46 (bs, *LW* = 13.8 Hz, T_1 = 39 ms, 2H, *H*10), 44.07 (bs, *LW* = 16.0 Hz, T_1 = 33 ms, 2H, *H*2), 36.26 (bs, *LW* = 14.1 Hz, T_1 = 55 ms, 2H, *H*5), 29.43 (bs, *LW* = 16.8 Hz, T_1 = 35 ms, 2H, *H*6), 23.63 (bs, *LW* = 11.4 Hz, T_1 = 85 ms, 2H, *H*4), 10.59 (bs, *LW* = 12.1 Hz, T_1 = 57 ms, 2H, *H*9), 7.14 (d, *J* = 6.8 Hz, T_1 = 848 ms, 8H, *H*14), 6.44 (d, *J* = 7.0 Hz, T_1 = 398 ms, 8H, H*13*), 3.40 (bs, *LW* = 10.5 Hz, T_1 = 124 ms, 4H, *H*12), 2.31 (bs, *LW* = 8.5 Hz, T_1 = 828 ms, 12H, *H*15), -0.75 (bs, *LW* = 11.7 Hz, T_1 = 78 ms, 2H, *H*3), -9.53 ppm (bs, *LW* = 72.6 Hz, T_1 = 19 ms, 4H, *H*11). **MS-ESI:** 1246.3338 ($[M\text{-}ClO_4]^+$, calcd. 1246.3343).

1.3.2 Synthesis of $[Zn(1)_2](ClO_4)_2$

According to the general procedure from **1** (350 mg, 0.64 mmol) and zinc(II) perchlorate hydrate (238 mg, 0.64 mmol) 162 mg of the title complex (44 % based on **1**) were obtained.

EA calcd. for $C_{74}H_{56}Cl_2N_8O_{10}Zn \cdot 3\ H_2O$ (%) C: 63.14, H: 4.44, N: 7.96; found C: 62.99, H: 4.05, N: 7.92. **^{1}H NMR** (500 MHz, d_3-MeCN, 300 K): 8.95 (d, *J* = 8.6 Hz, 2H, *H*6), 8.82 (d, *J* = 8.6 Hz, 2H, *H*7), 8.60 (dd, *J* = 8.2, 1.4 Hz, 2H, *H*1), 8.36 (d, *J* = 7.5 Hz, 2H, *H*8), 8.22 (d, *J* = 9.1 Hz, 2H, *H*5), 8.17 (d, *J* = 9.1 Hz, 2H, *H*4), 8.13 (dd, *J* = 4.8, 1.4 Hz, 2H, *H*3), 8.10 (t, *J* = 7.9 Hz, 2H, *H*9), 7.60 (dd, *J* = 8.2, 4.8 Hz, 2H, *H*2),

7.16 (d, *J* = 8.2 Hz, 8H, *H*14), 6.86 (d, *J* = 8.2 Hz, 8H, *H*13), 6.76 (d, *J* = 8.3 Hz, 2H, *H*10), 6.52 (d, *J* = 8.8 Hz, 4H, *H*12), 5.70 (d, *J* = 8.8 Hz, 4H, *H*11), 2.32 ppm (s, 12H, *H*15). **MS-ESI**: 1251.3297 ([M-ClO_4]$^+$, calcd. 1251.3292); 1252.3331 ([M+H-ClO_4]$^+$, calcd. 1252.3370).

1.3.3 Synthesis of [Fe(1)$_2$](ClO_4)$_2$

According to the general procedure from **1** (300 mg, 0.55 mmol) and iron(II) perchlorate hexahydrate (140 mg, 0.55 mmol) 210 mg of the title complex (58 % based on **1**) were obtained.

EA calcd. for $C_{74}H_{56}Cl_2FeN_8O_{10} \cdot H_2O$ (%) C: 65.26, H: 4.29, N: 8.23; found C: 65.45, H: 4.06, N: 8.22. **^{1}H NMR** (500 MHz, d_3-MeCN, 300 K): 42.30 (bs, *LW* = 1700 Hz, 2H, *H*1), 23.60 (bs, *LW* = 324 Hz, T_1 = 59 ms, 2H, *H*7), 19.65 (bs, *LW* = 230 Hz, T_1 = 62 ms, 2H, *H*2), 18.48 (bs, *LW* = 270 Hz, T_1 = 67 ms, 2H, *H*8), 16.77 (bs, *LW* = 161 Hz, T_1 = 71 ms, 2H, *H*10), 11.72 (bs, *LW* = 28 Hz, T_1 = 198 ms, 2H, *H*4), 11.09 (bs, *LW* = 22 Hz, T_1 = 160 ms, 2H, *H*9), 9.98 (d, *J* = 7.4 Hz, 2H, *H*5), 9.10 (bs, *LW* = 15 Hz, T_1 = 137 ms, 2H, *H*3), 7.03 (d, *J* = 8.1 Hz, T_1 = 971 ms, 8H, *H*13), 6.60 (d, *J* = 8.83 Hz, T_1 = 665 ms, 8H, *H*14), 6.18 (d, *J* = 4.6 Hz, T_1 = 286 ms, 4H, *H*11), 4.67 (bs, *LW* = 20 Hz, T_1 = 42 ms, 4H, *H*12), 3.00 (bs, *LW* = 71 Hz, T_1 = 118 ms, 2H, *H*6), 2.26 ppm (bs, *LW* = 3,5 Hz, T_1 = 834 ms, 12H, *H*15). **MS-ESI:** 1243.3358 ([M-ClO_4]$^+$, calcd. 1243.3361).

1.3.4 Synthesis of [Co(2)$_2$](BF_4)$_2$

According to the general procedure **2** (400 mg, 1.2 mmol) and cobalt(II) tetrafluoroborate hexahydrate (409 mg, 1.2 mmol) 376 mg of the title compound were obtained (67 % based on **2**).

EA calcd. for $C_{46}H_{30}B_2CoF_8N_6O_2 \cdot H_2O \cdot$ ½ MeCN (%) C 58.21, H: 3.48, N: 9.39; found C: 58.21, H: 3.38, N: 9.24. **^{1}H NMR** (500 MHz, d_3-MeCN, 300 K): 179.40 (bs, *LW* = 211.5 Hz, T_1 = 2.1 ms, 2H, *H*1), 116.55 (bs, *LW* = 55.8 Hz, T_1 = 13 ms, 2H, *H*7), 90.53 (bs, *LW* = 43.2 Hz, T_1 = 16 ms, 2H, *H*8), 44.96 (bs, *LW* = 15.3 Hz, T_1 = 51 ms, 2H, *H*10), 44.82 (bs, *LW* = 18.4 Hz, T_1 = 39 ms, 2H, *H*2), 35.36 (bs, *LW* = 14.8 Hz, T_1 = 68 ms, 2H, *H*5), 29.65 (bs, *LW* = 17.8 Hz, T_1 = 43 ms, 2H, *H*6), 22.04 (bs, *LW* = 11.4 Hz, T_1 = 111 ms, 2H, *H*4), 12.03 (bs, *LW* = 13.2 Hz, T_1 = 66 ms, 2H, *H*9), 4.10 (t, *J* = 6.7 Hz, T_1 = 315 ms, 2H, *H*13), 2.63 (bs, *LW* = 15.4 Hz, T_1 = 175 ms, 4H, *H*12), -2.65 (bs, *LW* = 12.0 Hz, T_1 = 110 ms, 2H, *H*3), -11.77 ppm (bs, *LW* = 48.3 Hz, T_1 = 23 ms, 4H, *H*11). **MS-ESI**: 844.1794 ([M-BF_4]$^+$, calcd. 844.1780).

1.3.5 Synthesis of [Co(2)$_2$](BF_4)$_3$

[Co(**2**)$_2$](BF_4)$_2$ (134 mg, 0.143 mmol) was dissolved in dry MeCN (3 mL). Nitrosyl tetrafluoroborate (25 mg, 0.214 mmol) was added and stirred for 3 h at room temperature. Et_2O was added until a precipitate was formed and centrifuged. The solid was washed with Et_2O and dried in vacuum to yield 140 mg of the title complex (96 % based on [Co(**2**)$_2$](BF_4)$_2$).

EA calcd. for $C_{46}H_{30}B_3CoF_{12}N_6O_2 \cdot$ ½ MeCN $\cdot$ 3 H_2O (%) C: 51.66, H: 3.46, N: 8.33; found C: 51.72, H: 3.21, N: 8.52. **^{1}H NMR** (500 MHz, d_3-MeCN, 300 K)*: 9.19 (d, *J* = 8.7 Hz, T_1 = 373 ms, 2H, *H*6), 8.97 (d, *J* = 8.7 Hz, T_1 = 210 ms, 2H, *H*7), 8.72 (d, *J* = 8.1 Hz, T_1 = 663 ms, 2H, *H*3), 8.45 (d, *J* = 9.0 Hz, T_1 = 489 ms, 2H, *H*5), 8.41 (d, *J* = 7.5 Hz, T_1 = 245 ms, 2H, *H*8), 8.37 (d, *J* = 8.9 Hz, T_1 = 610 ms, 2H, *H*4), 8.09 (t, *J* = 7.9 Hz, T_1 = 509 ms, 2H, *H*9), 7.58 (m, T_1 = 331 ms, 2H, *H*2), 7.28 (m, T_1 = 1 s, 6H, *H*12, *H*13), 7.18 (d, *J* = 5.4 Hz, T_1 = 162 ms, 2H, *H*1), 6.48 (d, *J* = 8.5 Hz, T_1 = 393 ms, 2H, *H*10), 6.16 (bs, T_1 = 282 ms, 4H, *H*11).

* T_1 times are determined by the self-exchange and therefore they are strongly influenced by Co^{2+} impurities, even if they are only percent small amounts < 0.1%.

1.3.6 Synthesis of [Co(3)$_2$](ClO_4)$_2$

2-(Pyridin-2-yl)-1,10-phenanthroline[1] (**3**) (200 mg, 0.78 mmol) was dissolved in a mixture of EtOH (5 mL) and CH_2Cl_2 (10 mL). To this solution $[Co(H_2O)_6](ClO_4)_2$ (200 mg, 0.6 mmol) dissolved in EtOH (3 mL) was added dropwise. The solution turned immediately brown and a precipitate formed. The precipitate was collected by centrifugation and washed with EtOH and Et_2O. The solid was dried in vacuum to yield $[Co(\mathbf{3})_2](ClO_4)_2$ (320 mg, 0.42 mmol) as brown-orange solid.

EA calcd. for $C_{34}H_{22}Cl_2CoN_6O_8$ (%) C: 52.87, H: 2.87, N: 10.88; found C: 52.37, H: 2.82, N: 11.17; **^{1}H NMR** (500 MHz, d_3-MeCN, 300 K): 134.79 (bs, *LW* = 162 Hz, T_1 = 2.4 ms, 2H, *H*1/11), 100.24 (bs, *LW* = 153 Hz, T_1 = 2.5 ms, 2H, *H*1/11), 85.69 (bs, *LW* = 27 Hz, T_1 = 19 ms, 2H, *H*7), 79.58 (bs, *LW* = 26 Hz, T_1 = 22 ms 2H, *H*8), 41.36(bs, *LW* = 14 Hz, T_1 = 40 ms, 2H, *H*2), 36.07 (bs, *LW* = 12 Hz, T_1 = 48 ms, 2H, *H*10), 32.15 (bd, *J* = 7 Hz, *LW* = 7 Hz, T_1 = 83 ms, 2H, *H*5), 26.36 (bs, *LW* = 12 Hz, T_1 = 58 ms, 2H, *H*6), 24.11 (bd, J = 7 Hz, *LW* = 7 Hz, T_1 = 112 ms, 2H, *H*4), 10.61 (bs, *LW* = 10 Hz, T_1 = 90 ms, 2H, *H*9), 4.43 ppm (bs, *LW* = 9 Hz, T_1 = 107 ms, 2H, *H*3).

$[Co(\mathbf{3})_2]^{3+}$ d_3-MeCN obtained by in situ oxidation using $(N(p\text{-}C_6H_4Br)_3)(SbCl_6)$: **^{1}H NMR** (500 MHz, d_3-MeCN, 300 K): 9.67 (d, *J* = 9.0 Hz, T_1 = 713 ms, 2H, *H*6), 9.31 (d, *J* = 8.7 Hz, T_1 = 505 ms, 2H, *H*7), 8.77 (d, *J* = 9.0 Hz, T_1 = 550 ms, 2H, *H*8), 8.72 (d, *J* = 8.7 Hz, T_1 = 890 ms, 2H, *H*3), 8.70 (d, *J* = 9.2 Hz, T_1 = 850 ms, 2H, *H*5), 8.47 (d, *J* = 9.0 Hz, T_1 = 900 ms, 2H, *H*4), 8.27 (td, *J* = 7.5, 1.3 Hz, T_1 = 830 ms, 2H, *H*9), 7.55 (dd, *J* = 5.6, 8.3 Hz, T_1 = 750 ms, 2H, *H*2), 7.35 (td, *J* = 6.0, 1.0 Hz, T_1 = 2.2 s, 2H, *H*11), 7.34 (dd, *J* = 6.0, 1.0 Hz, T_1 = 890 ms, 2H, *H*1), 7.31 ppm (dd, *J* = 6.0, 1.0 Hz, T_1 = 702 ms, 2H, *H*10).

1.3.7 Synthesis of $[Co(4)_2](BF_4)_2$

Complex $[Co(\mathbf{4})_2](BF_4)_2$ was prepared as described above.

EA calcd. for $C_{34}H_{20}B_2Br_2CoF_8N_6$ (%) C: 43.40, H: 2.57, N: 8.93; found C: 43.12, H: 2.55, N: 8.69. **^{1}H NMR** (500 MHz, d_3-MeCN, 300 K): 244.77 (bs, *LW* = 460 Hz, T_1 = 0.9 ms, 2H, *H*1), 141.61 (bs, *LW* = 116 Hz, T_1 = 6.3 ms, 2H, *H*7), 107.67 (bs, *LW* = 86 Hz, T_1 = 8 ms, 2H, *H*8), 50.57 (bs, *LW* = 20 Hz, T_1 = 20 ms 2H, *H*2), 34.68 (bs, *LW* = 14 Hz, T_1 = 31 ms, 2H, *H*10), 34.50 (bs, *LW* = 19 Hz, T_1 = 24 ms, 2H, *H*6), 31.96 (bs, *LW* = 44 Hz, T_1 = 45 ms, 2H, *H*5), 19.77 (bs, *LW* = 17 Hz, T_1 = 35 ms, 2H, *H*9), 14.14 (bs, *LW* = 10 Hz, T_1 = 103 ms, 2H, *H*4), -11.14 (bs, *LW* = 20 Hz, T_1 = 76 ms, 2H, *H*3). **MS-ESI**: 815.9473 ($[M\text{-}BF_4]^+$, calcd. 815.9466), 816.9481 ($[M+H\text{-}BF_4]^+$, calcd. 816.9545).

1.4 Electrochemical measurements

1.4.1 Cyclic voltammetry using *d* = 3 mm electrode

Cyclic voltammograms were recorded in acetonitrile solution of the compound (1 mM) with $[N(^nBu)_4][B(C_6F_5)_4]$ added as supporting electrolyte (100 mM) at v = 100 mV/s under argon atmosphere at 25°C. A three electrode cell, which utilised a Pt auxiliary electrode, a glassy carbon working electrode (3 mm diameter) and an Ag/Ag^+ (0.01 M $AgNO_3$) reference electrode mounted on a Luggin capillary was used. The working electrode was cleaned by polishing on a Buehler MicroFloc first with a 1 µm and then with a 1/4 µm diamond paste. All potentials were referenced internally to decamethylferrocene (-513 mV vs. ferrocene as internal standard). Potentials are given relative to ferrocene. The peak currents i_{pa}/i_{pc} for processes declared reversible were equal within the error of the setup.

Table 1-SI Peak potentials given for **1**, $[Co(\mathbf{1})_2](ClO_4)_2$, $[Zn(\mathbf{1})_2](ClO_4)_2$, $[Fe(\mathbf{1})_2](ClO_4)_2$, 4-methoxy-*N*,*N*-di-*p*-tolylaniline, $[Co(\mathbf{2})_2](BF_4)_2$ and $[Co(\mathbf{3})_2](ClO_4)_2$ at ambient temperature. $E^{0\prime}(M^{2+/3+})$ and $E^{0\prime\prime}$(Tara) are the redox potentials of the metal and the Tara unit. $\Delta E_p(M^{2+/3+})$ and ΔE_p(Tara) are the differences between the anodic and cathodic potentials of the metal and Tara redox event respectively.

Compound	$E^{0\prime}(M^{2+/3+})$ [mV]	$\Delta E_p(M^{2+/3+})$ [mV]	$E^{0\prime}$(Tara) [mV]	ΔE_p(Tara) [mV]
1	-	-	304	58
$[Co(\mathbf{1})_2](ClO_4)_2$	284	106	531	68
$[Zn(\mathbf{1})_2](ClO_4)_2$	-	-	473	76
$[Fe(\mathbf{1})_2](ClO_4)_2$	-	-	462	110
4-methoxy-*N*,*N*-di-*p*-tolylaniline	-	-	279	60
$[Co(\mathbf{2})_2](BF_4)_2$	265*	(340)*	-	-
$[Co(\mathbf{3})_2](ClO_4)_2$	98	180	-	-

* In case of $[Co(\mathbf{2})_2](BF_4)_2$ the value of $E_{pa}(M^{2+/3+})$ is difficult to define. Instead the onset potentials (described at **Table *3-SI***) were used to specify the redox potential $E^{0\prime}(M^{2+/3+})$ of the $Co^{2+/3+}$ redox process.

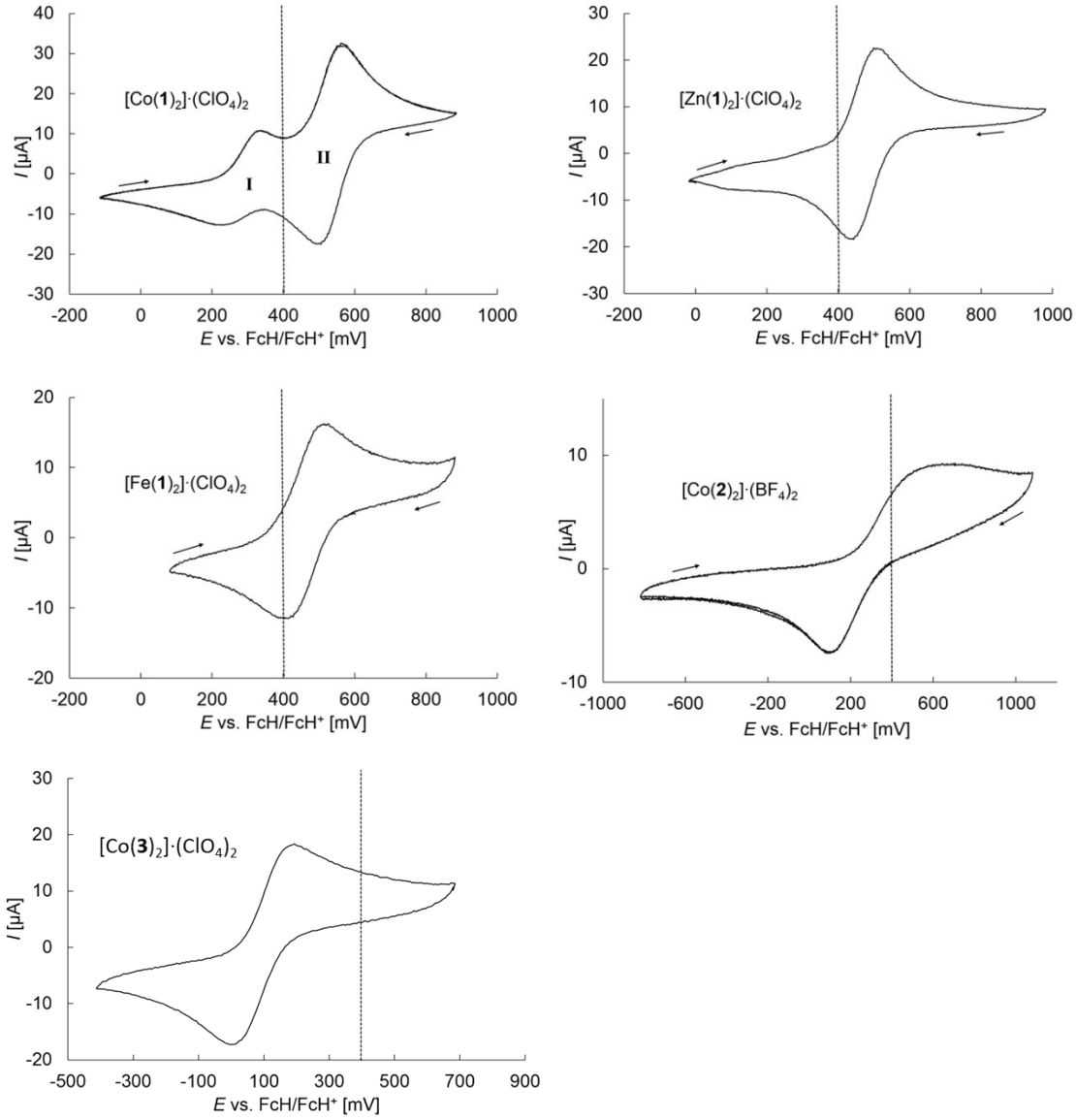

Figure 1-SI Cyclic voltammograms of $[Co(\mathbf{1})_2](ClO_4)_2$, $[Zn(\mathbf{1})_2](ClO_4)_2$, $[Fe(\mathbf{1})_2](ClO_4)_2$, $[Co(\mathbf{2})_2](BF_4)_2$ and $[Co(\mathbf{3})_2](BF_4)_2$. The dashed line at 400 mV is added as a guide to the eye. The CV of $[Co(\mathbf{1})_2](ClO_4)_2$ exhibits two separated redox events whereas the first one being the $Co^{2+/3+}$ and the second one being the $Tara^{0/+}$ centred redox process. In the $[Zn(\mathbf{1})_2](ClO_4)_2$ and $[Fe(\mathbf{1})_2](ClO_4)_2$ complexes the redox processes can be assigned to the $Tara^{0/+}$ redox couple while no metal centred redox process is visible. In $[Co(\mathbf{2})_2](BF_4)_2$ the oxidation process of Co^{2+} is hindered leading to difficulties of locating $E_{pa}(M^{2+/3+})$. The CV of $[Co(\mathbf{3})_2](ClO_4)_2$ shows one redox process which is assigned to $Co^{2+/3+}$ which is shifted to much smaller potential because of the missing substituents on the phenanthroline-pyridyl unit.

Cyclic voltammograms of $[Co(\mathbf{1})_2](ClO_4)_2$ were recorded at different temperatures. With decreasing temperature the difference in the redox potentials of both redox sites increases. The $Co^{2+/3+}$ redox process is substantially hindered at low temperatures. The oxidation is facilitated by a mediator effect of the amine.

Table 2-SI Peak potentials given for $[Co(\mathbf{1})_2](ClO_4)_2$ at different temperatures. E_{pa} is the anodic peak potential and E_{pc} is the cathodic peak potential. $E^{0\prime}(M^{2+/3+})$ and $E^{0\prime\prime}$(Tara) are the redox potentials of the metal and the Tara unit with their difference given by ΔE^0.

T [°C]	T [K]	$E_{pa}(M^{2+/3+})$ [mV]	$E_{pc}(M^{2+/3+})$ [mV]	$E^{0\prime}(M^{2+/3+})$ [mV]	E_{pa}(Tara) [mV]	E_{pc}(Tara) [mV]	$E^{0\prime\prime}$(Tara) [mV]	ΔE^0 [mV]
-19	254	345	55	200	553	477	515	315
-10	263	356	140	248	580	502	541	293
0	273	345	117	231	558	488	523	292
10	283	345	139	242	572	492	532	290
20	293	350	174	262	569	499	534	272
30	303	357	243	300	580	500	540	240
40	313	361	269	315	570	492	531	216
50	323	379	295	337	593	517	555	218

Table 3-SI Onset potentials given for $[Co(\mathbf{1})_2](ClO_4)_2$ at different temperatures. The onset potentials are the lowest (for the anodic reaction, E_a) or the highest (for the cathodic reaction, E_c) potentials at which the reaction product is formed. They are given for the metal ($M^{2+/3+}$) and Tara redox event and their arithmetic mean is the redox potential of the metal and Tara centred process, respectively.

T [°C]	T [K]	$E_a(M^{2+/3+})$ [mV]	$E_c(M^{2+/3+})$ [mV]	$E^{0\prime}(M^{2+/3+})$ [mV]	E_a(Tara) [mV]	E_c(Tara) [mV]	$E^{0\prime\prime}$(Tara) [mV]	ΔE^0 [mV]
-19	254	180	236	208	405	635	520	312
-10	263	186	314	250	414	688	551	301
0	273	190	298	244	408	668	538	294
10	283	189	309	249	409	665	537	288
20	293	190	330	260	420	670	545	285
30	303	188	376	282	420	684	522	270
40	313	211	377	294	425	691	558	264
50	323	225	409	317	437	705	571	254

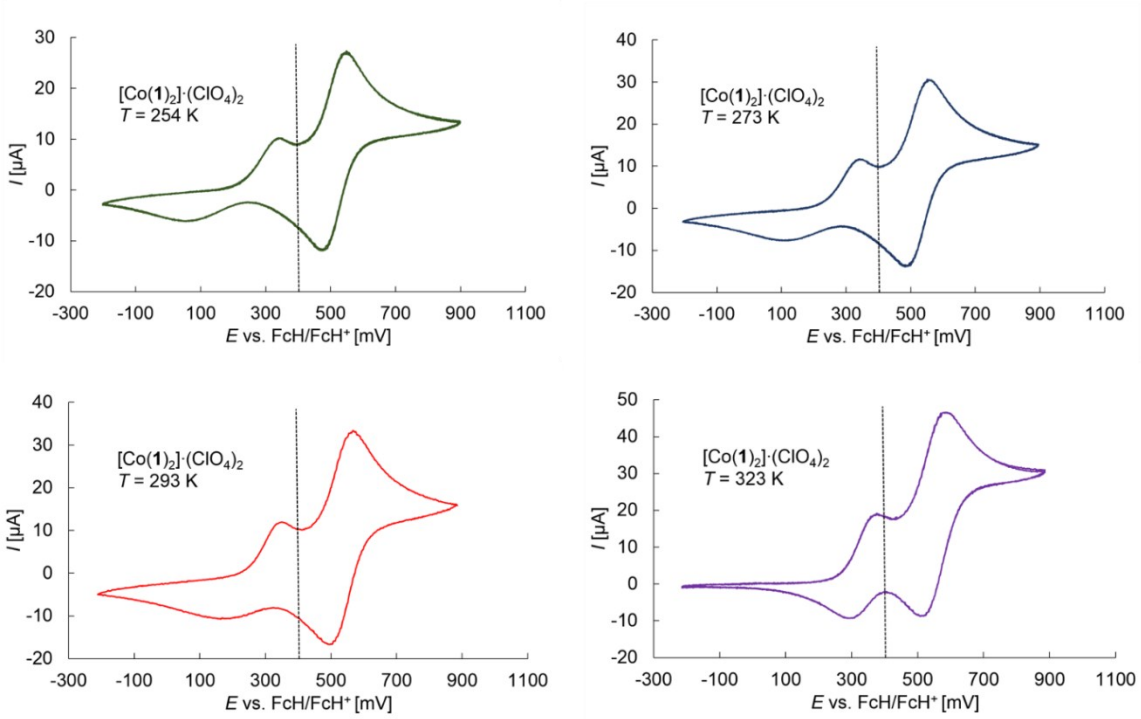

Figure 2-SI VT-CV of $[Co(\mathbf{1})_2](ClO_4)_2$ at given temperatures. The dashed line at 400 mV is added as a guide to the eye.

1.4.2 Cyclic voltammetry using a UME d = 18 µm electrode

CVs recoded on the UME (ultramicroelectrode) should serve as qualitative expansion of previous measurement on the conventional sized electrode. Therefore, a simplified setup was used, no corrections for solution resistance or double layer capacity were applied. The Ag electrode served as pseudo reference and no correction for a possible drift were applied. Cyclic voltammograms were measured in acetonitrile solution of the compound (≈ 5 mM) with $[N(^nBu)_4][B(C_6F_5)_4]$ added as supporting electrolyte (100 mM) under nitrogen atmosphere at 25°C. A two electrode cell, which utilised a Ag electrode formed as a pot to hold the solution (0.05 mL) and Pt working electrode (18 µm nominal diameter) was used. The working electrode was cleaned by polishing on a Buehler MicroFloc first with a 1 µm and then with a 1/4 µm diamond paste. **Figure *3-SI*** shows the recorded cyclic voltammograms.

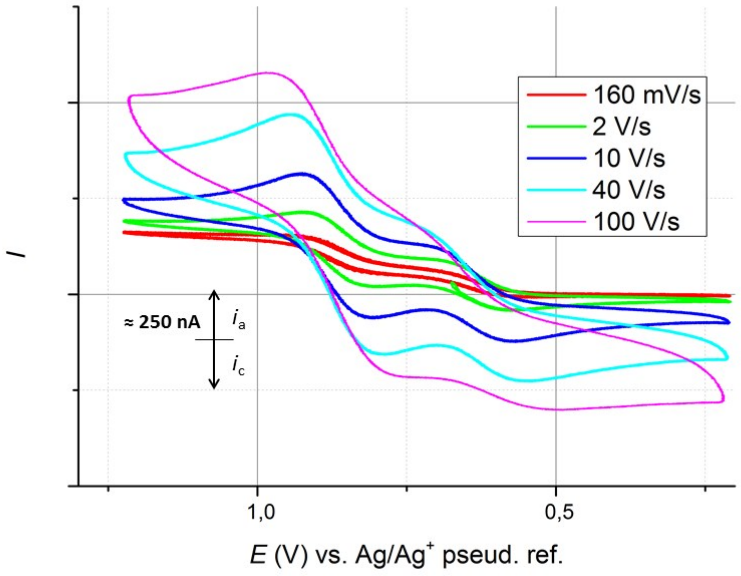

Figure 3-SI CVs of $[Co(\mathbf{1})_2](ClO_4)_2$ recorded in acetonitrile solution using a UME (*d* = 18 µm).

1.5 Structure determination - Single-crystal X-ray diffraction analysis

Crystals of $[Co(\mathbf{1})_2](BF_4)_2$ suitable for single crystal analysis were grown by slow diffusion of diethyl ether into a solution of the complex in MeCN. Data for $[Co(\mathbf{1})_2](BF_4)_2$ were collected at 110 K with graphite-monochromated Mo *Kα* radiation (*λ* = 0.71073 Å). The molecular structure was solved by direct methods using SHELXS-13[4] and refined by full-matrix least square procedures on F^2 using SHELXL-13[5,6] All non-hydrogen atoms were refined anisotropically.

H atoms were introduced at calculated positions and treated as riding on their parent atoms [*d*(CH) = 0.93 Å, *d*(CH_3) = 0.96 Å] with displacement parameters equal to 1.2 Ueq (C_6H_5) 1.5 Ueq (CH_3) times than the parent atom. Graphics for the molecular structures were created by using ORTEP[7].

Both BF_4^- counter ions have been refined on two sets of sites with occupancy ratios of 0.78:0.22 and 0.62:0.38. The crystal also contained solvent molecules. However, an appropriate refinement using two sets of sights remained unstable. Thus, the residual electron density referring to solvent

molecules has been removed by using the SQUEEZE[8] procedure included in the PLATON package.[9,10] The unit cell contained an omitted solvent accessible void of 1091.8 Å^3 that contained 145 electrons. Referring to the crystallization procedure this could correspond to 4 molecules of diethyl ether (= 42 electrons) per unit cell. This would result in a volume of 273 Å^3 per diethyl ether.

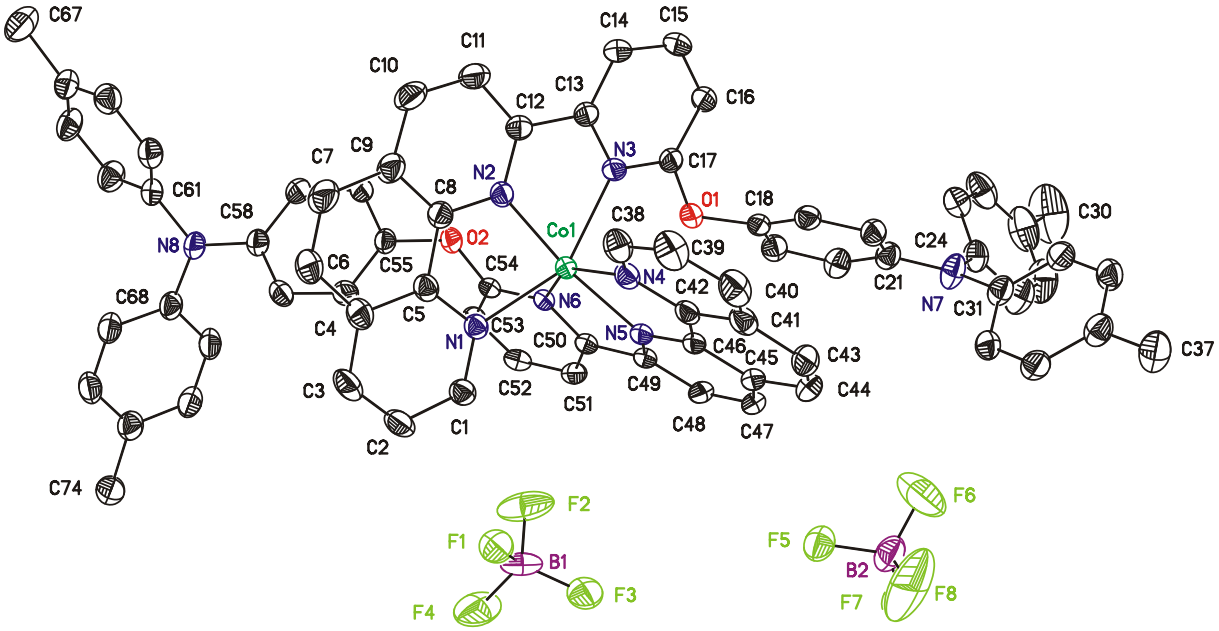

Figure 4-SI ORTEP (50 % probability level) of the structure of [Co(**1**)$_2$](BF$_4$)$_2$. Hydrogen atoms and disordered parts of molecules have been omitted for clarity.

Table 4-SI Crystal structure data of [Co(**1**)$_2$](BF$_4$)$_2$

	[Co(**1**)$_2$](BF$_4$)$_2$
empirical formula	$C_{74}H_{56}B_2CoF_8N_8O_2$
formula weight (g/mol)	1321.81
T (K)	110(2)
Wavelength (Å)	0.71073
crystal system, space group	Triclinic, *P*–1
unit cell dimensions	
a (Å)	13.3143(4)
b (Å)	13.8274(5)
c (Å)	23.1341(6)
α (°)	91.825(2)
β (°)	97.651(2)
γ (°)	110.463(3)
Volume (Å^3)	3940.6(2)
Z	2
absorption coefficient (mm^{-1})	0.281
F(000)	1362
crystal size (mm^3)	0.2 x 0.05 x 0.02
Θ-range f. data coll. (°)	2.994 – 26.000
limiting indices	-16 ≤ *h* ≤ 16, -17 ≤ *k* ≤ 17, -28 ≤ *l* ≤ 28
reflections coll. / unique	49598/15446 [R_{int} = 0.0267]
Completeness to *Θ* = 25° (%)	99.7 %
absorption correction	Semi-empirical from equivalents

max. and min. transmission	1.00000 and 0.90167
data / restraints / parameters	15448/40/932
GooF on F^2	1.045
final *R* indices ($I > 2\sigma(I)$)	*R*1 = 0.0526, *wR*2 = 0.1437
R indices (all data)	*R*1 = 0.0643, *wR*2 = 0.1504
larg. diff. peak and hole ($e^-/Å^3$)	0.680 and -0.728

Table 5-SI: Selected bond lengths and angles for $[Co(\mathbf{1})_2](BF_4)_2$.

$[Co(\mathbf{1})_2](BF_4)_2$	Bond lengths /Å
Co – N(1)	2.1619(17)
Co – N(2)	2.0413(18)
Co – N(3)	2.2125(16)
Co – N(4)	2.1987(18)
Co – N(5)	2.0493(18)
Co – N(6)	2.1759(17)
N(2)-Co-N(5)	168.54(7)
N(2)-Co-N(1)	77.01(7)
N(5)-Co-N(1)	108.07(7)
N(2)-Co-N(6)	116.45(7)
N(5)-Co-N(6)	74.60(7)
N(1)-Co-N(6)	85.54(6)
N(2)-Co-N(4)	92.30(7)
N(5)-Co-N(4)	76.85(7)
N(1)-Co-N(4)	99.33(6)
N(6)-Co-N(4)	151.13(7)
N(2)-Co-N(3)	74.65(7)
N(5)-Co-N(3)	101.50(6)
N(1)-Co-N(3)	150.17(7)
N(6)-Co-N(3)	98.84(6)
N(4)-Co-N(3)	90.95(6)

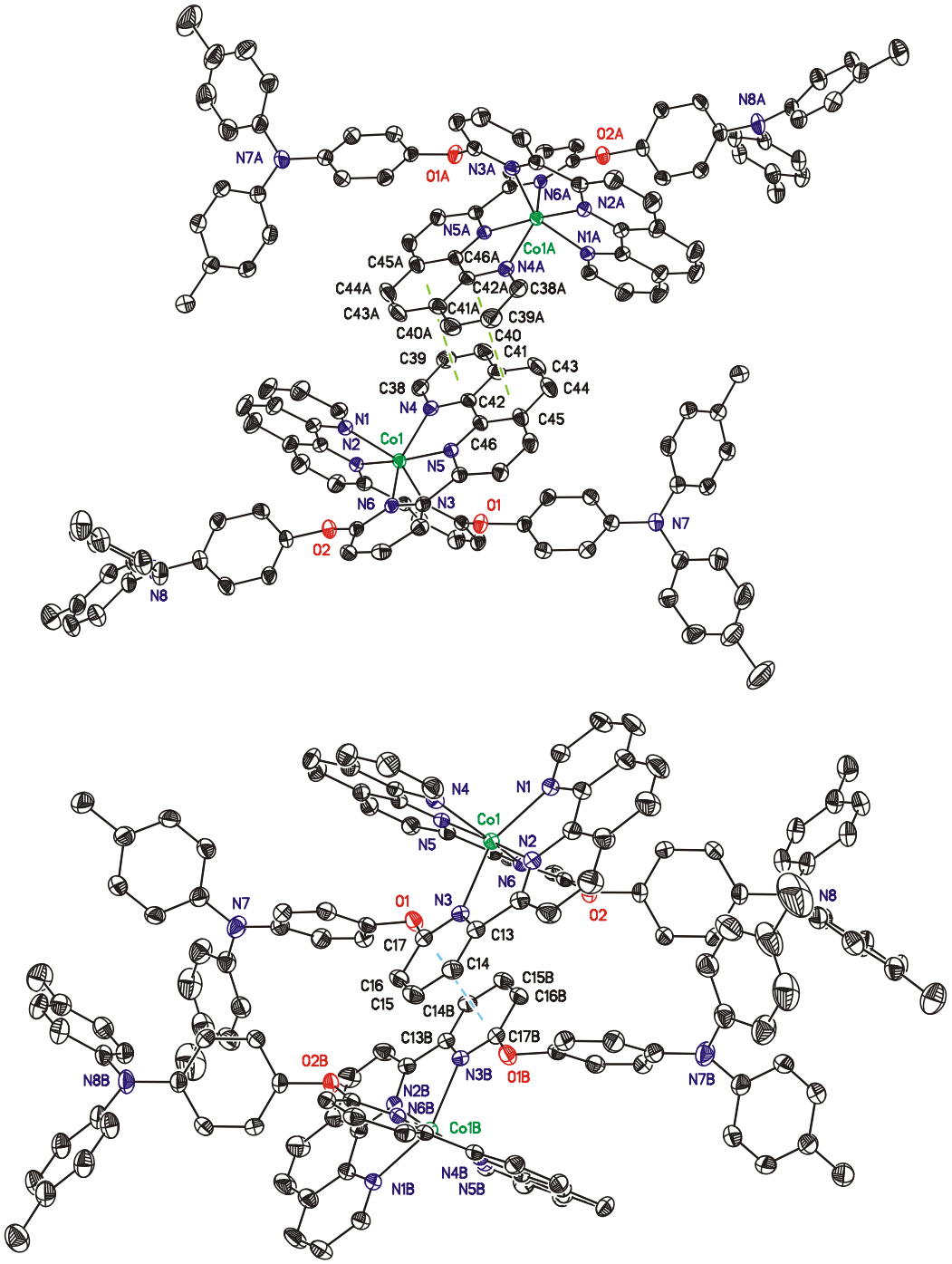

Colour	Distance / Å	Plane intersection	Symmetry operation
green	4.4637(15)[a)]	0°	(A) –x, –y, 2–z
blue	3.6533(13)	0.43(11)°	(B) 1–x, 1–y, 2–z

Figure 5-SI: ORTEP (50 % probability level) of the molecular structure of $[Co(\mathbf{1})_2](BF_4)_2$ showing intermolecular parallel (displaced) π-π interactions (green, blue). Hydrogen atoms, the complete labelling and counter ions have been omitted for clarity. a) Slippage: 2.633 Å.

Table 6-SI: *C···F Distances within the sum of the van-der-Waals radii (∑ = 3.17 Å) in the packing of compound [Co(**1**)$_2$](BF$_4$)$_2$.*

D–H···A	H···A / Å	D···A / Å	D–H···A	Symmetry Operation
C1–H1···F1	2.53	3.066(4)	117 °	–
C2–H2···F1	2.52	3.049(5)	116 °	–
C14–H14···F3	2.42	3.162(3)	137 °	X, –1+y, z
C23–H23···F4	2.44	3.096(4)	128 °	–x, 1–y, 2–z
C39–H39···F5	2.47	3.028(4)	119 °	1–x, 1–y, 2–z
C52–H52···F5	2.37	3.150(5)	141 °	–x, 1–y, 2–z

The D–H distance has been fixed at 0.93 Å

1.6 EPR/UV-vis-NIR spectroelectrochemical experiments

The EPR/UV-vis-NIR spectroelectrochemical technique was described earlier.[11] For EPR measurements, an EMX X-band CW spectrometer (Bruker BioSpin, Germany) was used. The EPR spectra were registered at a microwave power of 2 mW and 100 kHz modulation. The EPR spectra were recorded in an optical EPR cavity (4104OR, Bruker, Germany) allowing the connection of two optical wave guides to measure *in situ* the electronic absorption spectra in transmission mode simultaneously with the EPR spectra. For UV-vis-NIR measurements, the spectrometers AvaSpec-2048x14-USB2 with the CCD detector and AvaSpec-NIR256-2.2 with the InGaAs detector (Avantes, The Netherlands) applying the AvaSoft7.5 software were used. For the *in situ* experiments a balanced deuterium-halogen lamp AvaLight-DH-S-BAL serves as the light source. The *in situ* spectroelectrochemical measurements were controlled by a PG 390 potentiostat/galvanostat (HEKA Elektronik GmbH, Germany) equipped with the PotMaster v2x80 software, triggering both the EPR and UV-vis-NIR spectrometer modules. In variable temperature experiments the temperature was controlled and maintained by a variable temperature controller.

The spectroelectrochemical experiments were carried out in an EPR flat cell with a three-electrode arrangement consisting of a gold-µ-mesh (99.9%, Goodfellow, UK) as the working electrode, a silver chloride-coated silver wire as the pseudo-reference electrode, and a platinum wire as the counter electrode. The potentials are given versus pseudo reference electrode. The EPR and vis-NIR spectra were collected at a continuous potential sweep rate of 5 mV/s. Each spectrum was collected relative to that of the neutral compound at the initial potential.

The concentration of the samples was 1 mM. Solutions of 0.1 M [N(^{n}Bu)$_4$][B(C$_6$F$_5$)$_4$][12,13] in acetonitrile (99.8%, anhydrous, Sigma-Aldrich) were used as electrolyte. The electrolyte was deaerated by nitrogen bubbling. The preparation of the solutions was done in glove box under inert atmosphere.

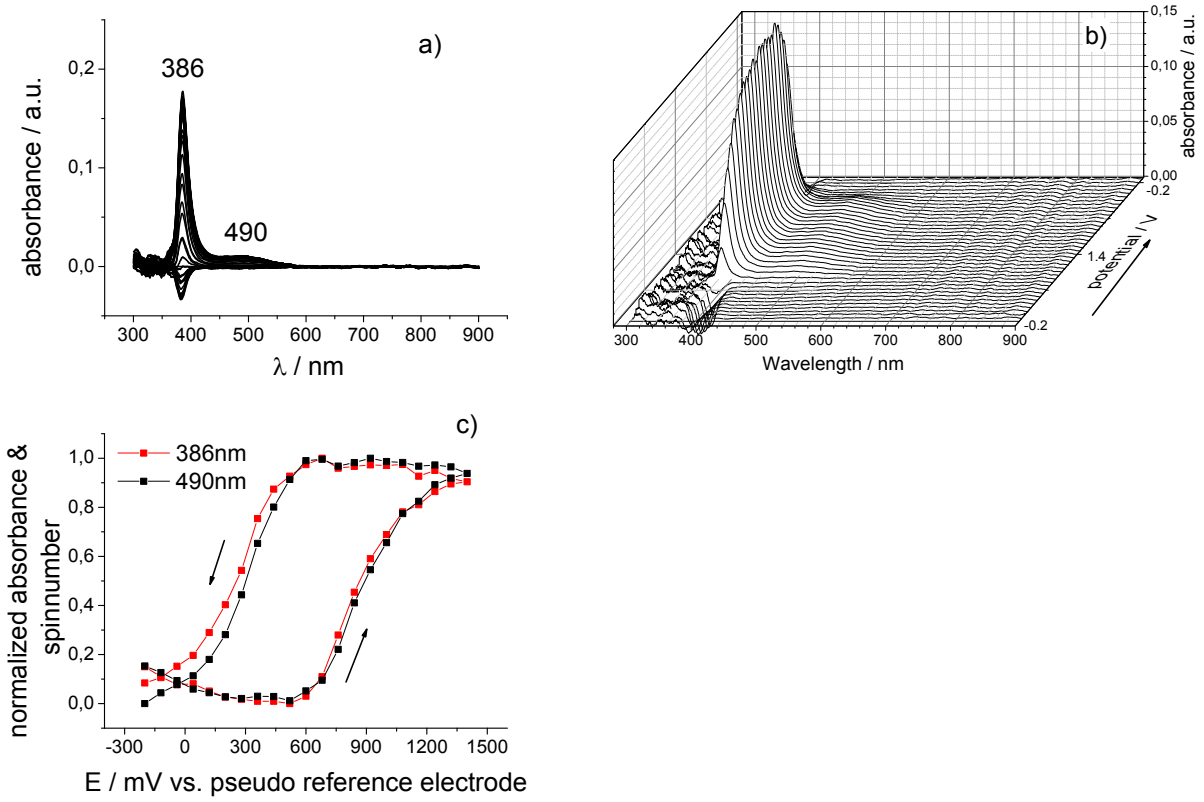

Figure 6-SI: UV-vis-NIR spectra of $[Co(\mathbf{2})_2](BF_4)_2$ in MeCN at 25°C, 2D plot (a) and 3D plot (b). Potential dependence of the absorption bands (c). The increasing absorption at 386 nm with a small shoulder at 490 nm is caused by the cobalt centred oxidation $Co^{2+/3+}$.

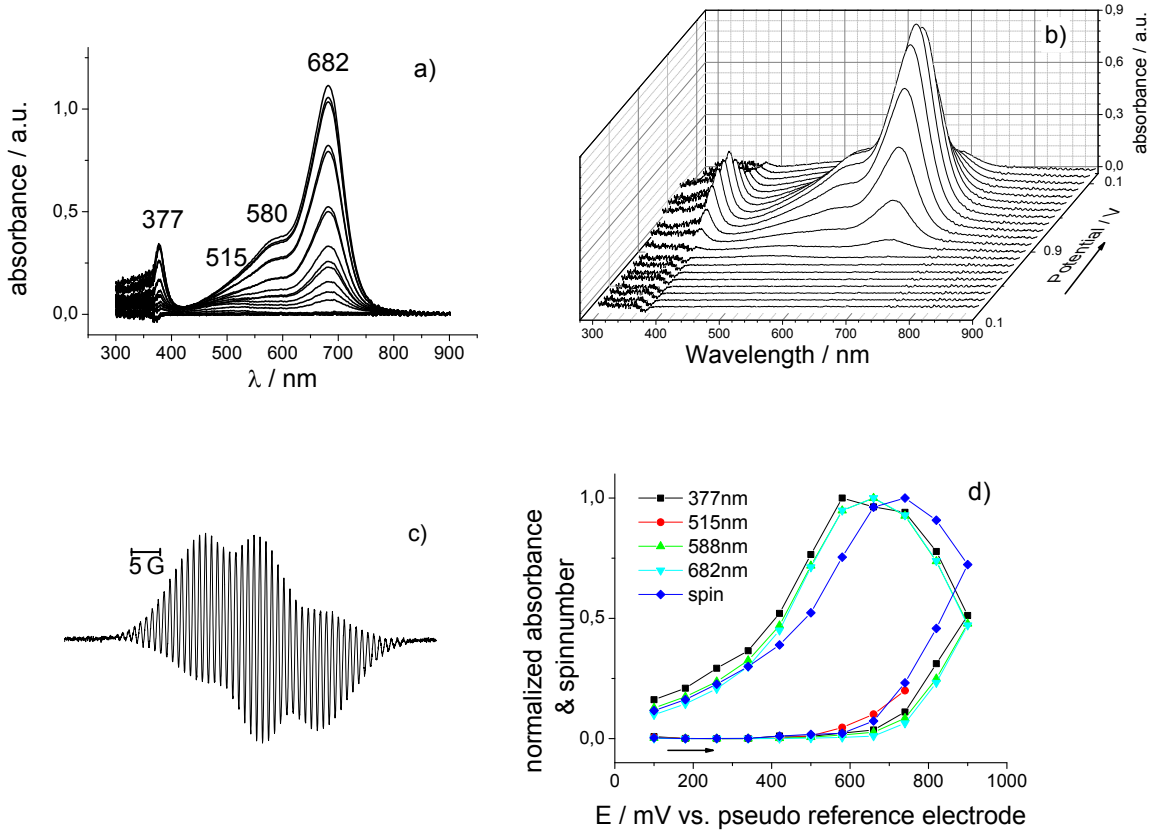

Figure 7-SI UV-vis-NIR spectra of $[Zn(\mathbf{1})_2](ClO_4)_2$ in MeCN at 25°C, 2D plot (a) and 3D plot (b). The rising absorption at 377 and 682 nm with shoulders at 515 and 580 nm are caused by the Tara oxidation and are characteristic for Tara$^+$ radical cations.[14] The EPR spectrum of $[Zn(\mathbf{1}^+)_2]^{4+}$ (c) and relative changes in the absorbance (UV-vis) and spin count (EPR) in dependence of potential.

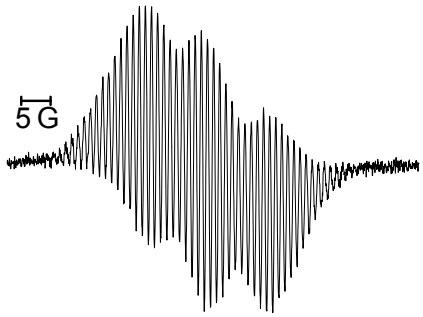

Figure 8-**SI** EPR spectrum of $[Fe(\mathbf{1})_2]^{2+}$ (1 mM) partially oxidized (0.5 equiv.) $[Fe(\mathbf{1}^+)_2]^{4+}$ (1 mM).

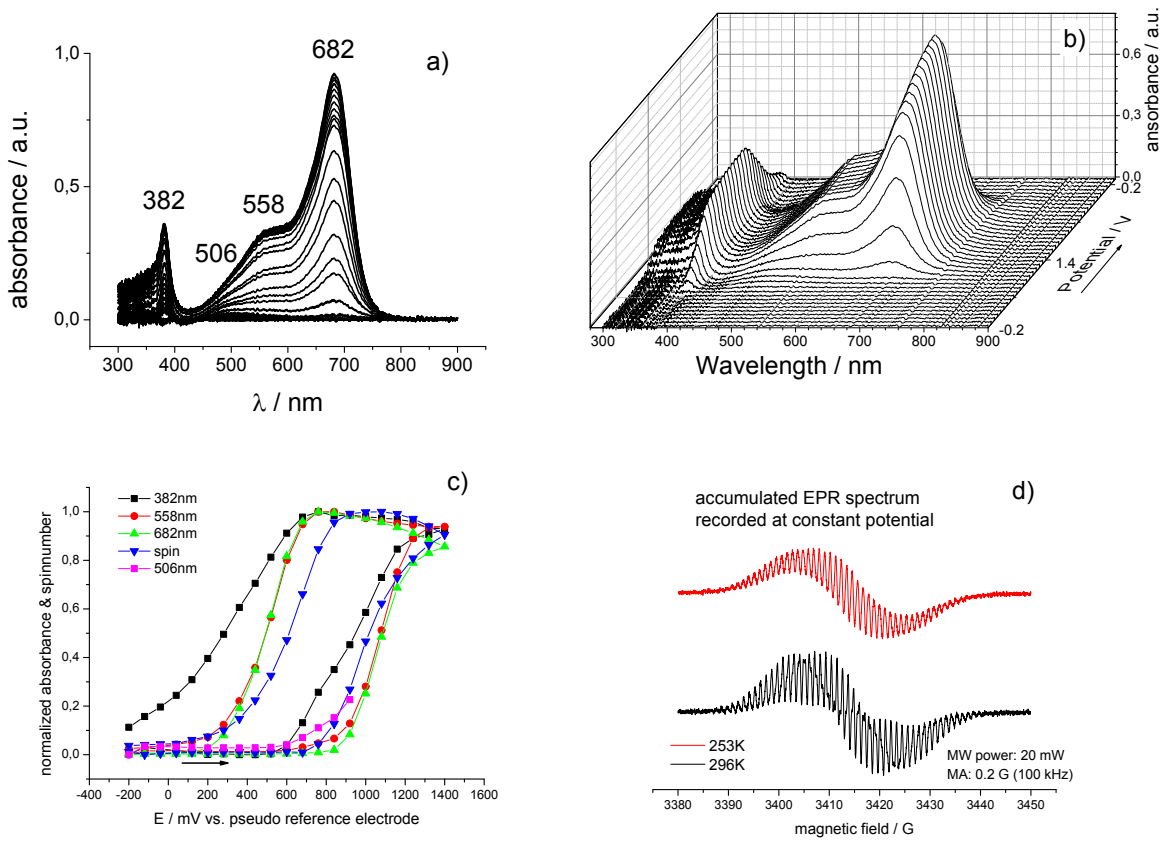

Figure 9-**SI:** In situ absorption spectra of $[Co(\mathbf{1})_2](BF_4)_2$, 2D plot (a) and 3D plot (b). Potential dependence of the absorption bands and EPR intensity (c). EPR spectrum recorded at different temperatures (d).

1.7 UV-vis-NIR-spectroscopy

The spectroelectrochemical UV-vis-NIR measurements of the complexes (2 mM) were performed in dry acetonitrile solutions. $[N^nBu_4][B(C_6F_5)_4]$ (0.1 M) was used as supporting electrolyte. Measurements were carried out in an OTTLE (= optically transparent thin-layer electrode, quartz windows for UV-vis-NIR) cell with a Varian Cary 5000 spectrophotometer at 25°C. Between the spectroscopic measurements the applied potentials have been increased step-wisely using step-heights of 25, 50, 100, 150, 200 or 300 mV. Afterwards the analyte was reduced at -300 mV and an additional spectrum was recorded to prove the reversibility of the oxidation.

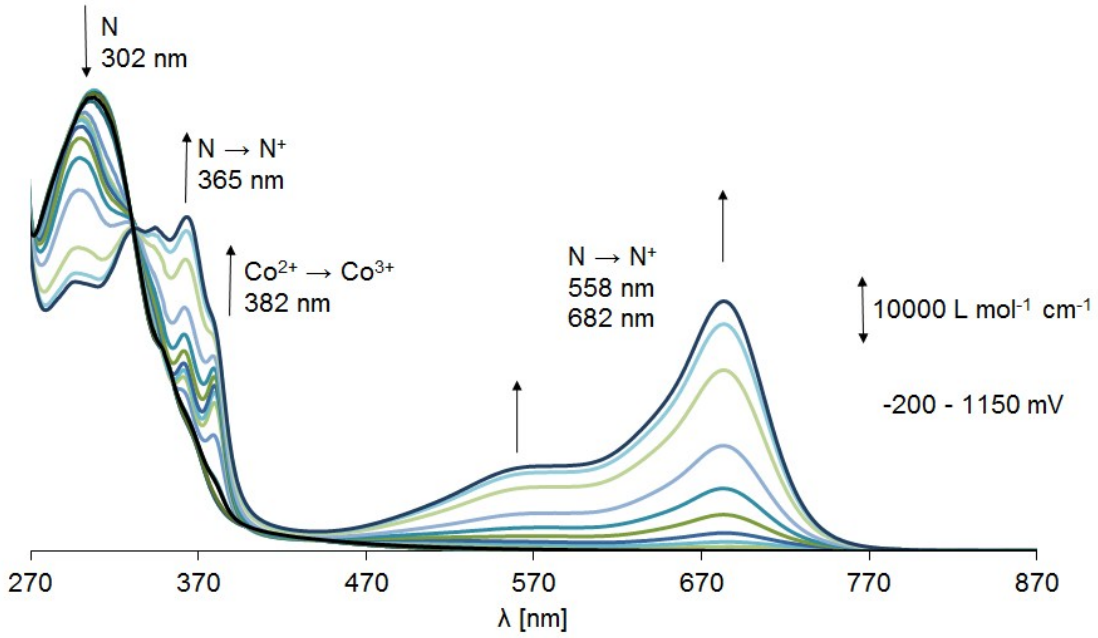

Figure 10-SI UV-vis-NIR spectra of $[Co(\mathbf{1})_2](ClO_4)_2$ in MeCN at 25°C. The black line is the additional recorded spectra at -300 mV to prove the reversibility of the oxidation. The spectra is dominated by the increasing absorbance of the positively charged nitrogen between 470 and 770 nm which is formed by the second oxidation process in $[Co(\mathbf{1})_2](ClO_4)_2$. There is no charge transfer band visible in the NIR region due to the poor electronic coupling of the Co^{3+} and Tara substituents in $[Co^{3+}(\mathbf{1})_2]^{3+}$.

1.8 ^{1}H NMR spectroscopy

All spectra were recorded on a Bruker Avance III 500 spectrometer including a TopSpin 2.1 programme package for data acquisition and processing. All spectra were referenced to $CDCl_3$ (^{1}H NMR δ = 7.26 ppm, ^{13}C NMR δ = 77.16 ppm) and to d_3-MeCN (^{1}H NMR δ = 1.96 ppm). The assignment of the signals of the compounds was based on the coupling pattern, ^{1}H,^{1}H-COSY spectroscopy, T_1 relaxation measurements and classical assignment rules. Intramolecular distances between a proton and the metal ion were approximated with respective Co-H distances taken from the single crystal structure analysis of the cobalt complex $[Co(\mathbf{1})_2](BF_4)_2$.

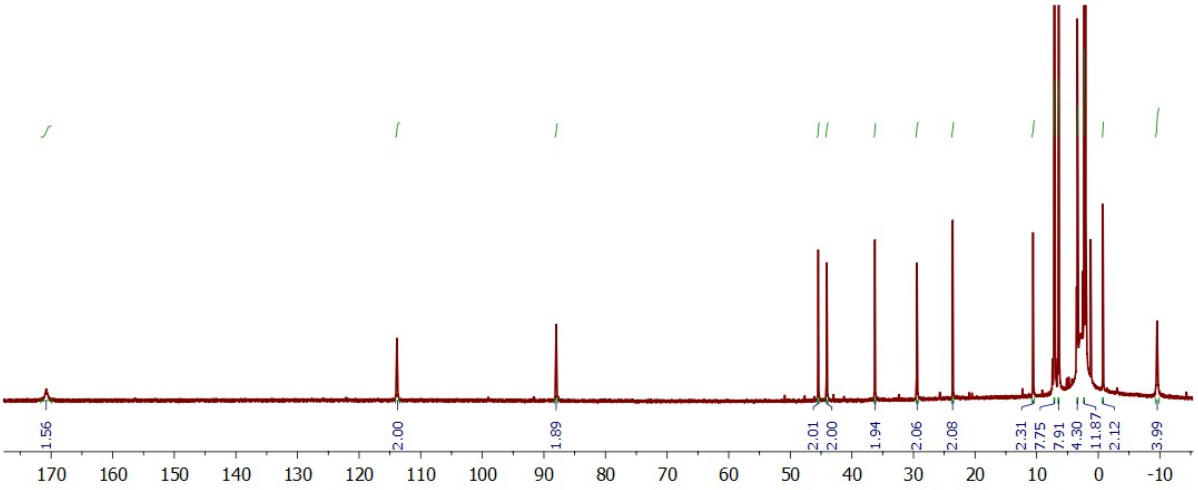

Figure 11-SI ^{1}H NMR spectra of $[Co(\mathbf{1})_2](ClO_4)_2$ in d_3-MeCN at 25°C.

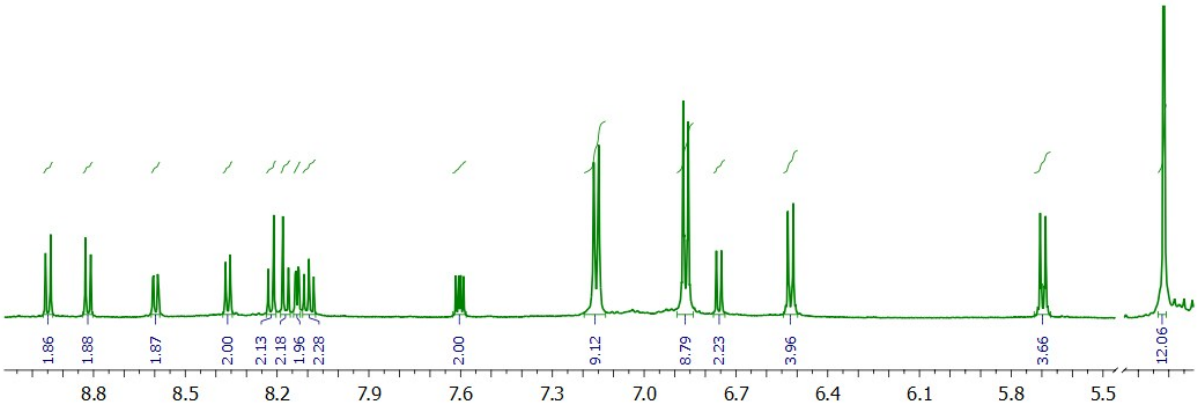

Figure 12-SI ^{1}H NMR spectra of $[Zn(\mathbf{1})_2](ClO_4)_2$ in d_3-MeCN at 25°C.

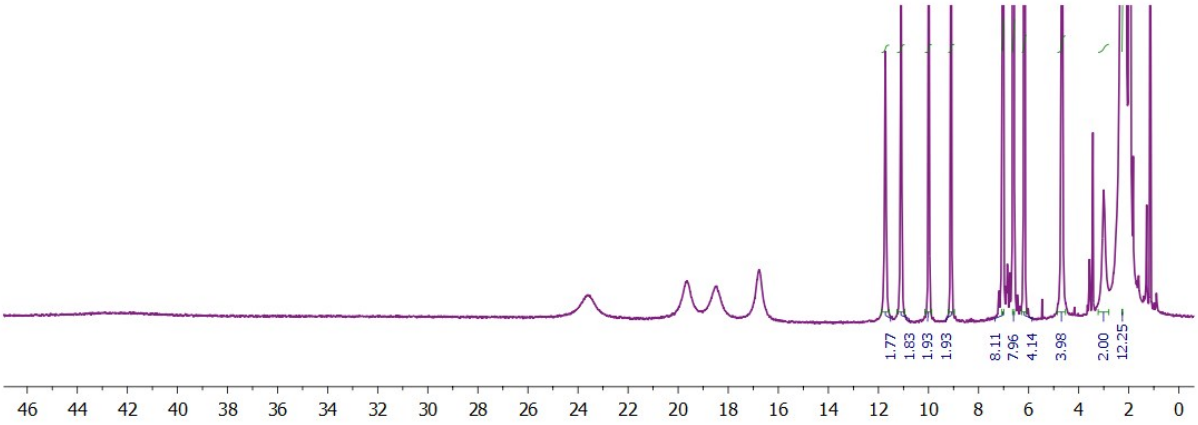

Figure 13-SI ^{1}H NMR spectra of [Fe(**1**)$_2$](ClO$_4$)$_2$ in d_3-MeCN at 25°C. Integrals for δ = 42.30, 23.60, 19.65, 18.48 and 16.77 ppm are not shown due to difficulties of the baseline correction resulting unrealistic number of protons.

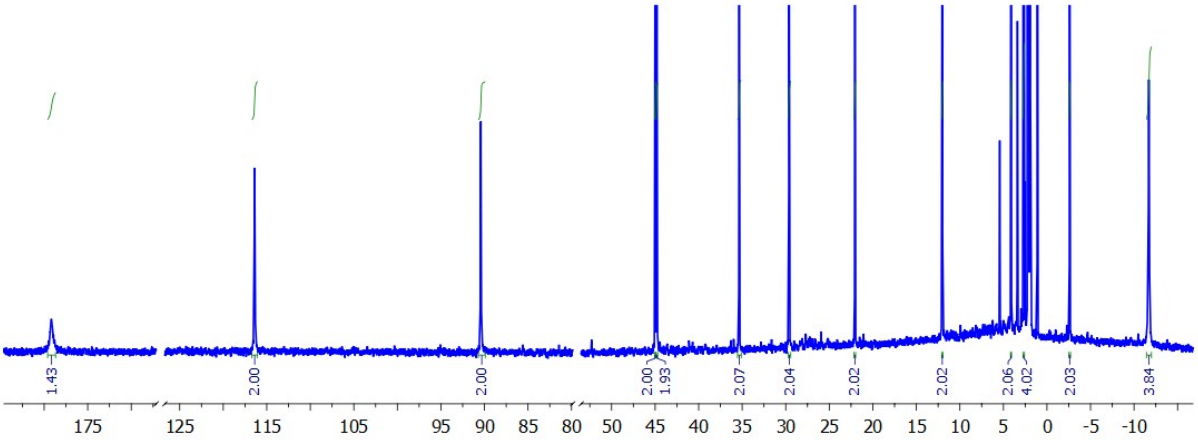

Figure 14-SI ^{1}H NMR spectra of [Co(**2**)$_2$](BF$_4$)$_2$ in d_3-MeCN at 25°C.

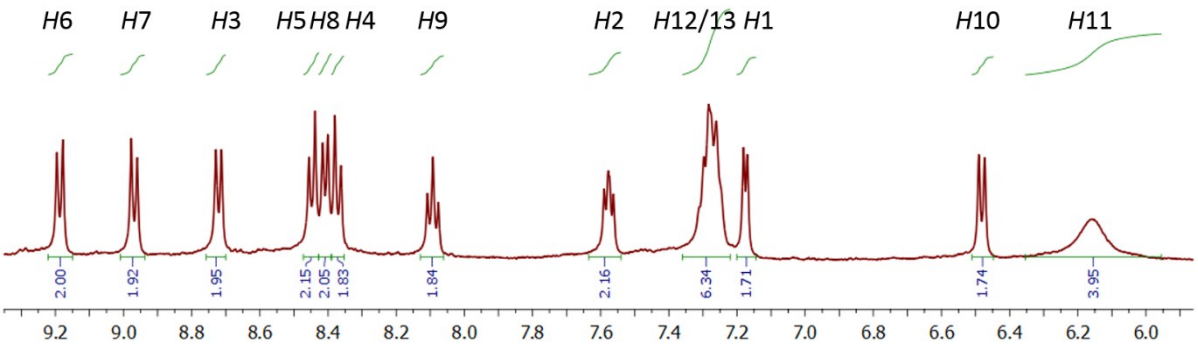

Figure 15-SI ^{1}H NMR spectra of [Co(**2**)$_2$](BF$_4$)$_3$ in d_3-MeCN at 25°C.

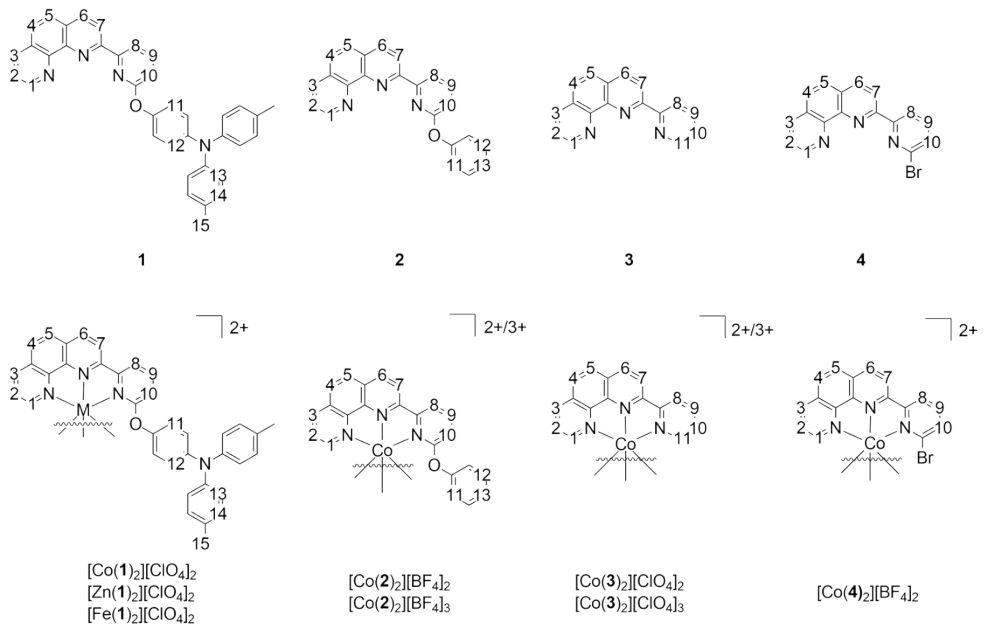

Figure 16-SI Position numbering scheme for protons used in discussion of NMR spectra and compound characterization.

Table 7-SI Assignment of protons in compounds **1** and **2**

	***δ* [ppm]**	
H	**1**	**2**
1	9.25	9.23
2	7.65	7.65
3	8.27	8.27
4	7.80	7.78
5	7.84	7.81
6	8.61	8.55
7	8.31	8.27
8	8.75	8.77
9	7.89	7.87
10	6.94	6.94
11	7.13	7.47 – 7.42
12	7.13	7.29 – 7.24
13	7.09/7.04	7.29 – 7.24
14		-
15	2.32	-

Table 8-SI Assignment of protons in compounds $[Co(\mathbf{1})_2](ClO_4)_2$, $[Zn(\mathbf{1})_2](ClO_4)_2$ and $[Fe(\mathbf{1})_2](ClO_4)_2$

	***δ* [ppm]**		
H	$[Co(\mathbf{1})_2](ClO_4)_2$	$[Zn(\mathbf{1})_2](ClO_4)_2$	$[Fe(\mathbf{1})_2](ClO_4)_2$
1	170.76	8.60	42.30
2	44.07	7.60	19.65
3	-0.75	8.13	9.10
4	23.63	8.17	11.72
5	36.26	8.22	9.98
6	29.43	8.95	3.00
7	113.86	8.82	23.60
8	88.00	8.36	18.48

9	10.59	8.10	11.09
10	45.46	6.76	16.77
11	-9.53	5.70	6.18
12	3.40	6.52	4.67
13	6.44	6.86	7.03
14	7.14	7.16	6.60
15	2.31	2.32	2.26

Table 9-SI Assignments of protons of compounds $[Co(\mathbf{2})_2](BF_4)_2$, $[Co(\mathbf{2})_2](BF_4)_3$, $[Co(\mathbf{3})_2](ClO_4)_2$, $[Co(\mathbf{3})_2](ClO_4)_3$ and $[Co(\mathbf{4})_2](BF_4)_2$

	***δ* [ppm]**				
H	$[Co(\mathbf{2})_2](BF_4)_2$	$[Co(\mathbf{2})_2](BF_4)_3$	$[Co(\mathbf{3})_2](ClO_4)_2$	$[Co(\mathbf{3})_2](ClO_4)_3$	$[Co(\mathbf{4})_2](BF_4)_2$
1	179.40	7.18	134.79/100.24	7.34	244.77
2	44.82	7.58	41.36	7.55	50.57
3	-2.65	8.72	4.43	8.72	-11.14
4	22.04	8.37	24.11	8.47	14.14
5	35.36	8.45	32.15	8.70	31.96
6	29.65	9.19	26.36	9.67	34.50
7	116.55	8.97	85.69	9.31	141.61
8	90.53	8.41	79.58	8.77	107.67
9	12.03	8.09	10.61	8.27	19.76
10	44.96	6.48	36.07	7.31	34.68
11	-11.77	6.16	134.79/100.24	7.35	-
12	2.63	7.28	-	-	-
13	4.10	7.28	-	-	-

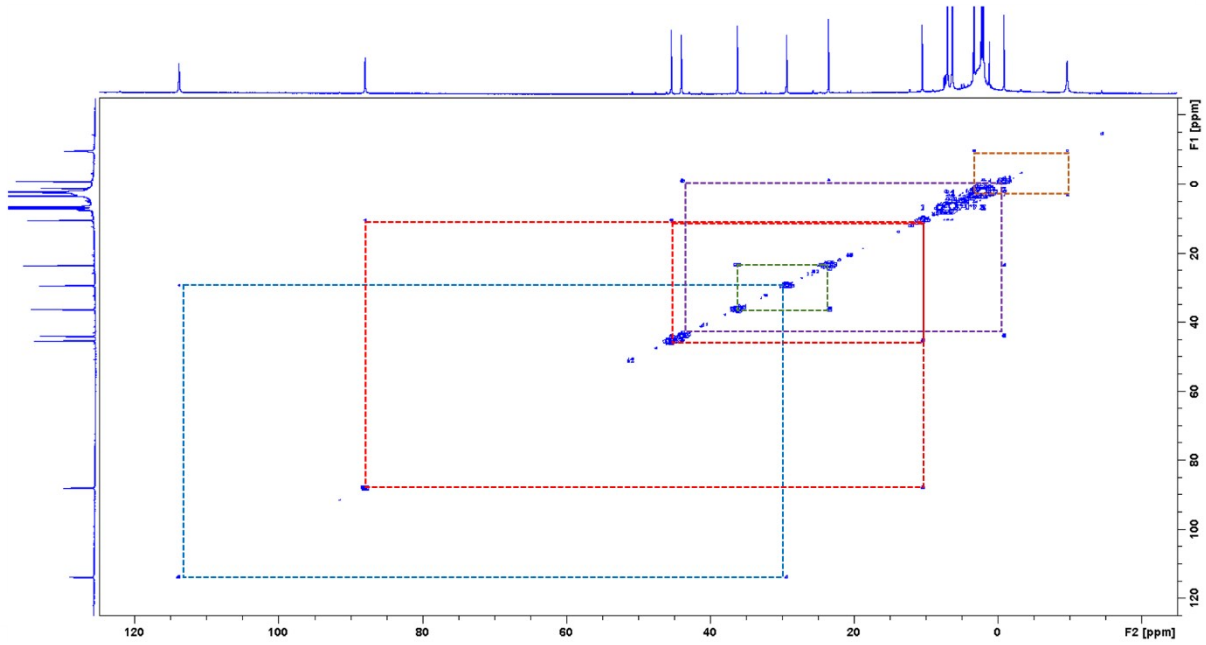

Figure 17-SI $^1H,^1H$-COSY of $[Co(\mathbf{1})_2](ClO_4)_2$ in d_3-MeCN at 25°C

Table 10-SI NMR data of $[Co(\mathbf{1})_2](ClO_4)_2$

Proton	δ [ppm]	d(Co-H) [Å]	T_1 [ms]	$R_1 = 1/T_1$ [ms^{-1}]	$1/d^6$ [$Å^{-6}$]
1	170.76	3.267	1.4	0.7143	$8.224 \cdot 10^{-4}$
2	44.07	5.208	33	0.0305	$5.012 \cdot 10^{-5}$
3	-0.75	5.864	78	0.0128	$2.459 \cdot 10^{-5}$
4	23.63	6.212	85	0.0118	$1.740 \cdot 10^{-5}$
5	36.26	6.185	55	0.0181	$1.786 \cdot 10^{-5}$
6	29.43	5.731	35	0.0285	$2.822 \cdot 10^{-5}$
7	113.86	5.007	12	0.0870	$6.347 \cdot 10^{-5}$
8	88.00	5.015	15	0.0676	$6.286 \cdot 10^{-5}$
9	10.59	5.866	57	0.0175	$2.454 \cdot 10^{-5}$
10	45.46	5.222	39	0.0255	$4.931 \cdot 10^{-5}$
11	-9.53	4.544	19	0.0532	$1.136 \cdot 10^{-4}$
12	3.40	6.785	124	0.0081	$1.025 \cdot 10^{-5}$
13	6.44	8.184	398	0.0025	$3.328 \cdot 10^{-6}$
14	7.14	9.985	848	0.0012	$1.009 \cdot 10^{-6}$
15	2.31	11.720	828	0.0012	$3.859 \cdot 10^{-7}$

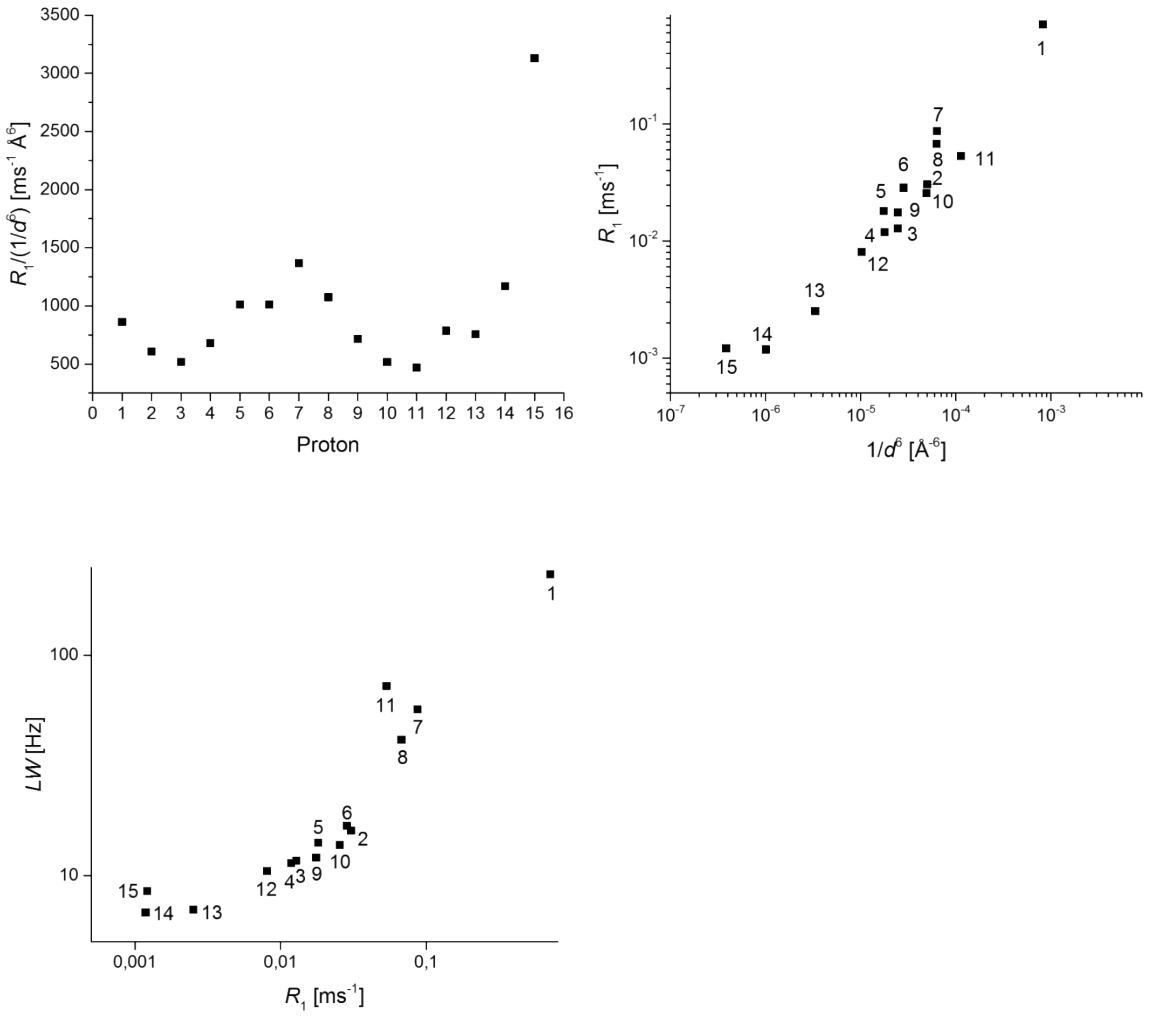

Figure 18-SI Results of the ^{1}H NMR spectroscopy on [Co(**1**)$_2$](ClO$_4$)$_2$. top left) The variating ratio between R_1 and $1/d^6$ indicates an anisotropic susceptibility which also becomes apparent in the strong different chemical shifts for *H*2/*H*10 (≈45 ppm) and *H*7/*H*8 (≈ 100 ppm). However the ratio R_1/R_2 is within the error of the experiment constant. This indicates an orientation independent electron relaxation time. top right) Plot of the R^1 vs $1/d^6$ the linear dependence indicate mainly dipolar coupling. button left) Plot of the $LW = R^2/\pi$ vs $1/d^6$ the linear dependence indicate mainly dipolar coupling.

Table 11-SI NMR data of [Fe(**1**)$_2$](ClO$_4$)$_2$

Proton	δ [ppm]	d (Co-H) [Å]	T_1 [ms]	$R_1 = 1/T_1$ [ms^{-1}]	$1/d^6$ [Å^{-6}]
1	42.30	3.267	--	--	$8.224\cdot10^{-4}$
2	19.65	5.208	62	0.016129	$5.012\cdot10^{-5}$
3	9.10	5.864	137	0.0072993	$2.459\cdot10^{-5}$
4	11.72	6.212	198	0.0050607	$1.740\cdot10^{-5}$
5	9.98	6.185	189	0.005291	$1.786\cdot10^{-5}$
6	3.00	5.731	118	0.0084746	$2.822\cdot10^{-5}$
7	23.60	5.007	59	0.0169492	$6.347\cdot10^{-5}$
8	18.48	5.015	67	0.0149254	$6.286\cdot10^{-5}$
9	11.09	5.866	160	0.00625	$2.454\cdot10^{-5}$
10	16.77	5.222	71	0.0140845	$4.931\cdot10^{-5}$
11	6.18	4.544	286	0.0034965	$1.136\cdot10^{-4}$
12	4.67	6.785	42	0.0238095	$1.025\cdot10^{-5}$
13	7.03	8.184	971	0.0010299	$3.328\cdot10^{-6}$
14	6.60	9.985	665	0.0015038	$1.009\cdot10^{-6}$

15	2.26	11.720	834	0.001199	$3.859 \cdot 10^{-7}$

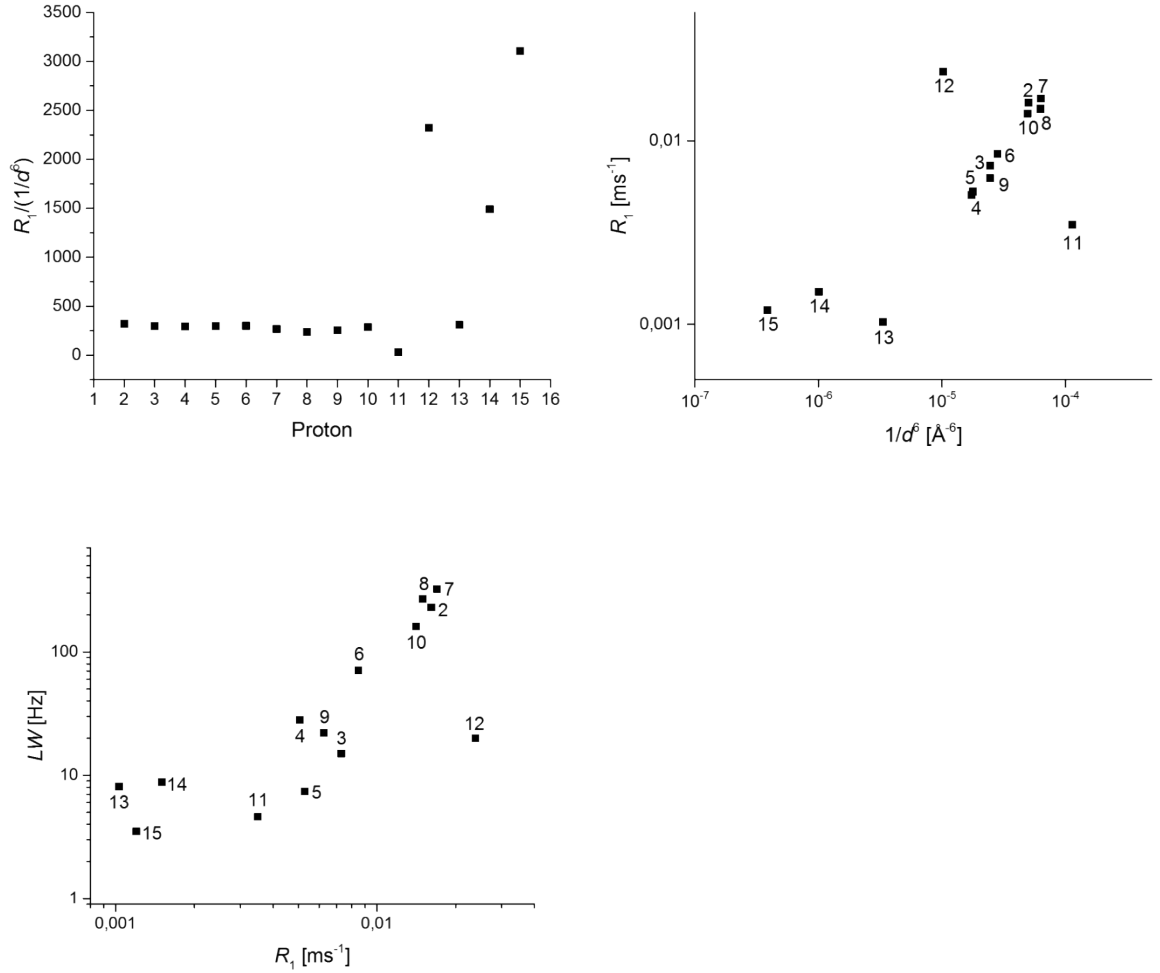

Figure 19-SI Results of ^{1}H-NMR spectroscopic investigations on [Fe(**1**)$_2$](ClO$_4$)$_2$. top left) plot of the distance dependent relaxivity R_1 the constant ratio for the rigid part indicates an orientation independent magnetic moment and electron relaxation time. top right) Plot of the R^1 vs $1/d^6$ the linear dependence indicate mainly dipolar coupling. button left) Plot of the $LW = R^2/\pi$ vs $1/d^6$ the linear dependence indicate mainly dipolar coupling.

Table 12-SI NMR data of [Co(**2**)$_2$](BF$_4$)$_2$

Proton	***δ* [ppm]**	***d* (Co-H) [Å]**	**T_1 [ms]**	**$R_1 = 1/T_1$ [ms^{-1}]**	**$1/d^6$ [Å^{-6}]**
1	179.40	3.267	2.1	0.4878	$8.224 \cdot 10^{-4}$
2	44.82	5.208	39	0.0256	$5.012 \cdot 10^{-5}$
3	-2.65	5.864	110	0.0091	$2.459 \cdot 10^{-5}$
4	22.04	6.212	111	0.0090	$1.740 \cdot 10^{-5}$
5	35.36	6.185	68	0.0148	$1.786 \cdot 10^{-5}$
6	29.65	5.731	43	0.0232	$2.822 \cdot 10^{-5}$
7	116.55	5.007	13	0.0794	$6.347 \cdot 10^{-5}$
8	90.53	5.015	16	0.0636	$6.286 \cdot 10^{-5}$
9	12.03	5.866	66	0.0152	$2.454 \cdot 10^{-5}$
10	44.96	5.222	51	0.0196	$4.931 \cdot 10^{-5}$
11	-11.77	4.544	23	0.0049	$1.136 \cdot 10^{-4}$
12	2.63	6.785	175	0.0057	$1.025 \cdot 10^{-5}$
13	4.10	---	315	0.0032	---

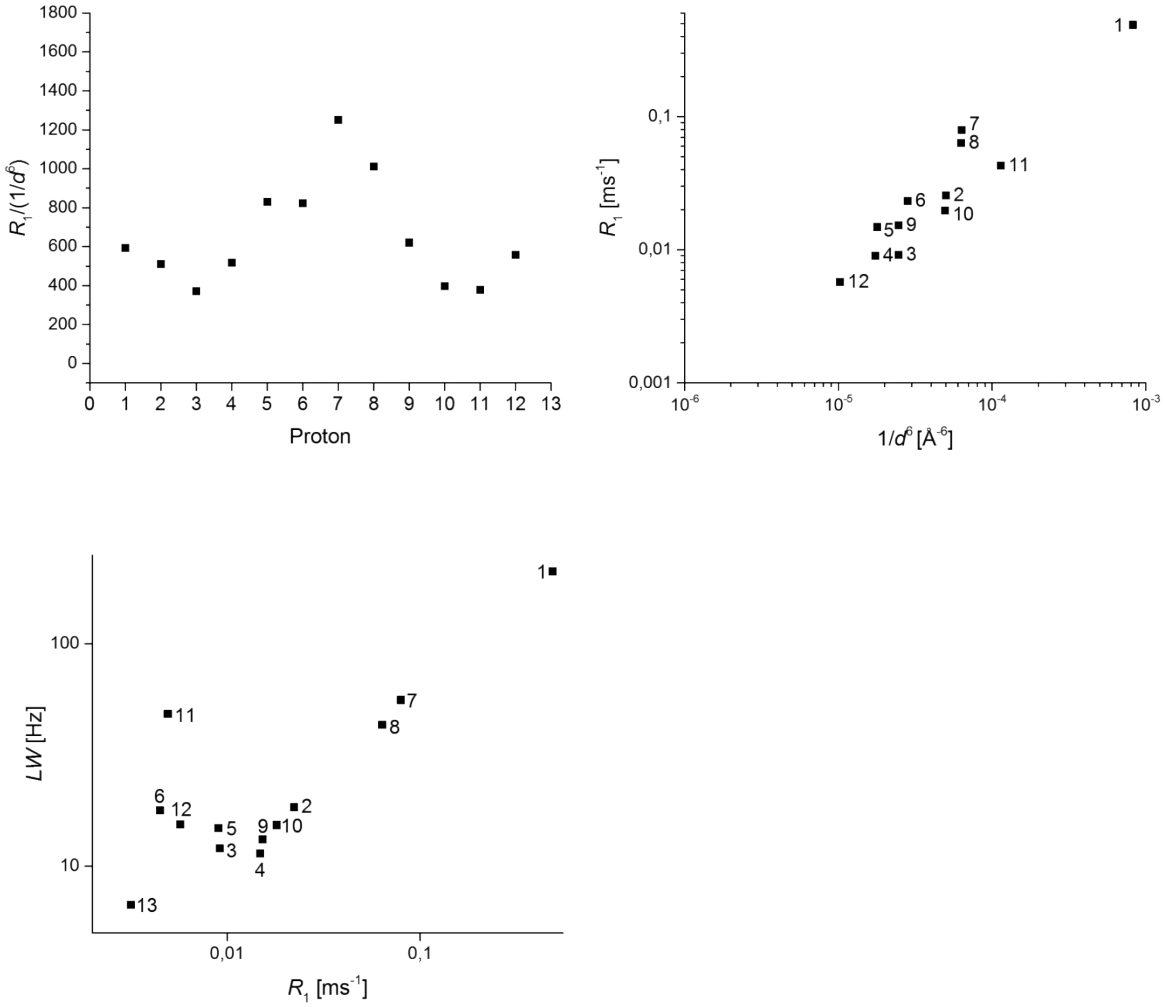

Figure 20-SI Results of the ^{1}H NMR spectroscopy on [Co(**2**)$_2$](BF$_4$)$_2$. top left) The variating ratio between R_1 and $1/d^6$ indicates an anisotropic susceptibility which also becomes apparent in the strong different chemical shifts for *H*2/*H*10 (≈ 45 ppm) and *H*7/*H*8 (≈ 100 ppm). However the ratio R_1/R_2 is constant within the errors of the experiment. This indicates an orientation independent electron relaxation time. top right) Plot of the R^1 vs. $1/d^6$ the linear dependence indicate mainly dipolar coupling. button left) Plot of the LW = R^2/π vs. $1/d^6$ the linear dependence indicate mainly dipolar coupling.

1.8.1 Assignment of proton resonances of the Co^{2+} complexes by tracking of the Co^{2+}/Co^{3+} self-exchange using EXSY NMR spectroscopy

The assignment of proton resonances in paramagnetic complexes can often be achieved by interpretation of the relaxivities $R_{1/2}$ together with ^{1}H,^{1}H-COSY-spectroscopy. Due to the mainly dipolar character of the coupling between protons and the unpaired electrons the longitudinal relaxivities R_1 are related to the distance of the proton to the metal by the relation $R_1 \sim d^{-6}$. This rule is almost perfectly fulfilled for the rigid parts of [Fe(**1**)$_2$]$^{2+}$ (**Figure *19-SI***), although it is a SCO complex (*vide infra*). For the Co^{2+} complexes [Co(**1**/**2**)$_2$]$^{2+}$ this rule does not apply (**Figure *18-SI*** and **Figure *20-SI***). The reason is likely an anisotropic susceptibility. The relaxivity of a proton in the vicinity of a paramagnetic metal is proportional to the square of the coupling energy, a dipolar coupling in this case. The coupling energy itself is proportional to the magnetic moment of the metal ion which is in case of an anisotropic susceptibility direction dependent. Octahedral complexes of Co^{2+} are well known for strong anisotropic susceptibilities. This impedes using the above mentioned relation.

Although ^{1}H,^{1}H-COSY-spectroscopy can give useful information for the assignment of the protons it is not sufficient to achieve full assignment.

An interesting method was published by Constable *et al.* [15] on the example of $[Co^{2+/3+}(terpy)_2]^{2+}$ they use the self-exchange in the redox couple $[Co^{2+/3+}(terpy)_2]^{2+/3+}$ to track the proton resonances from the diamagnetic Co^{3+} complex to the paramagnetic Co^{2+} complex by selective EXSY spectroscopy. [15] The method was not straightforwardly transferable to Co complexes in this series. The reasons are likely the rather fast electron relaxation times T_1 ($1/R_1$) in the HS-Co^{2+} state. Selective pulses that are used to excite the paramagnetic resonances are rather long (0.1 < ms to tens of seconds); resonances with a T_1 time of a few ms are difficult to excite by this method. In addition Bruker's selective EXSY uses z-gradients to select the desired coherences. Z-gradients are usually also in the order of ms. During these delays the magnetisation is relaxed and lost before the acquisition time starts. However, the largest problem is the slower self-exchange. For example if T_1 for a particular proton is 10 ms and the self-exchange rate is 50 M s^{-1} in a 10 mM solution, 30 ms after the inverting pulse 92% of the z-magnetisation is relaxed to the equilibrium but only 1.3% is transferred to the Co^{3+} state. Therefore the self-exchange must be increased by the addition of a redox catalyst. In this case we used acetylferrocene/-ferrocenium ($E^{o\prime}$ ≈ 270 mV vs. Fc)[16] for the couple $[Co^{2+/3+}(\mathbf{3})_2]^{2+/3+}$ and a triarylamine/-aminium ($Tara^{0/+}$) couple (4-methoxy-*N,N*-di-*p*-tolylaniline ($E^{o\prime}$ = 250 mV vs. Fc))[14] for the couple $[Co^{2+/3+}(\mathbf{2})_2]^{2+/3+}$ (self-exchange for ferrocene/ferrocenium and triarylamines/aminium are about 10^6 M s^{-1}).[17] With this method the self-exchange could be accelerated to occur on the ms time scale as indicated by the linewidths of Co^{3+} resonance and the dramatically shorter T_1 times for the Co^{3+} resonances. (***Figure 26-SI*** and ***Figure 28-SI***)

With this improvement we were able to use the 2D version of the EXSY experiment (p1 = 15 µs). In addition, the pulse program with a classical phase cycle was used avoiding z-gradients. The mixing time was set to 30 ms and reasonable spectra (***Figure 24-SI*** and ***Figure 25-SI*** for $[Co(\mathbf{2})_2]^{2+/3+}$) were observed within few minutes (relaxation delay d1 = 300 ms). The spectra are not free of artefacts but artefacts are clearly detectable by a lack of the second symmetry equivalent cross peak. The disadvantage of the method is the increased complexity of sample preparation and the decreased resolution due to the increased T_2 time of the Co^{3+} resonances. However we found a sufficient number of correlations to give an almost full assignment of all resonances of the paramagnetic Co^{2+} complexes. The determination of T_1 values is shown and described in **Figure *26-SI***.

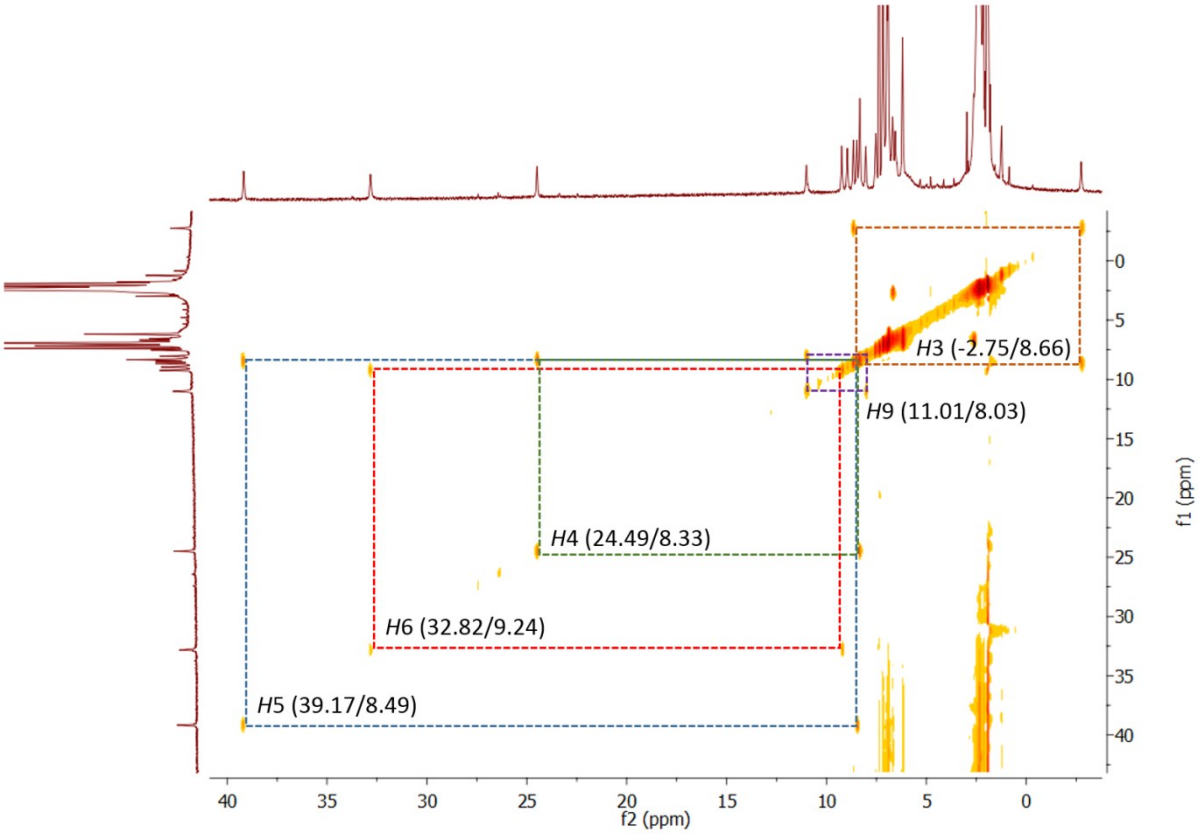

Figure 21-SI Section of $^{1}H,^{1}H$-EXSY-NMR spectra of $[Co(\mathbf{1})_2]^{2+}$ which is partly oxidised to $[Co(\mathbf{1})_2]^{3+}$ by adding a substoichiometric amount (≈ 0.5 eq) of "magic blue" at 273 K. The values given in brackets are the chemical shifts in ppm for the Co^{2+} and Co^{3+} species respectively. Mixing time was set to 100 ms.

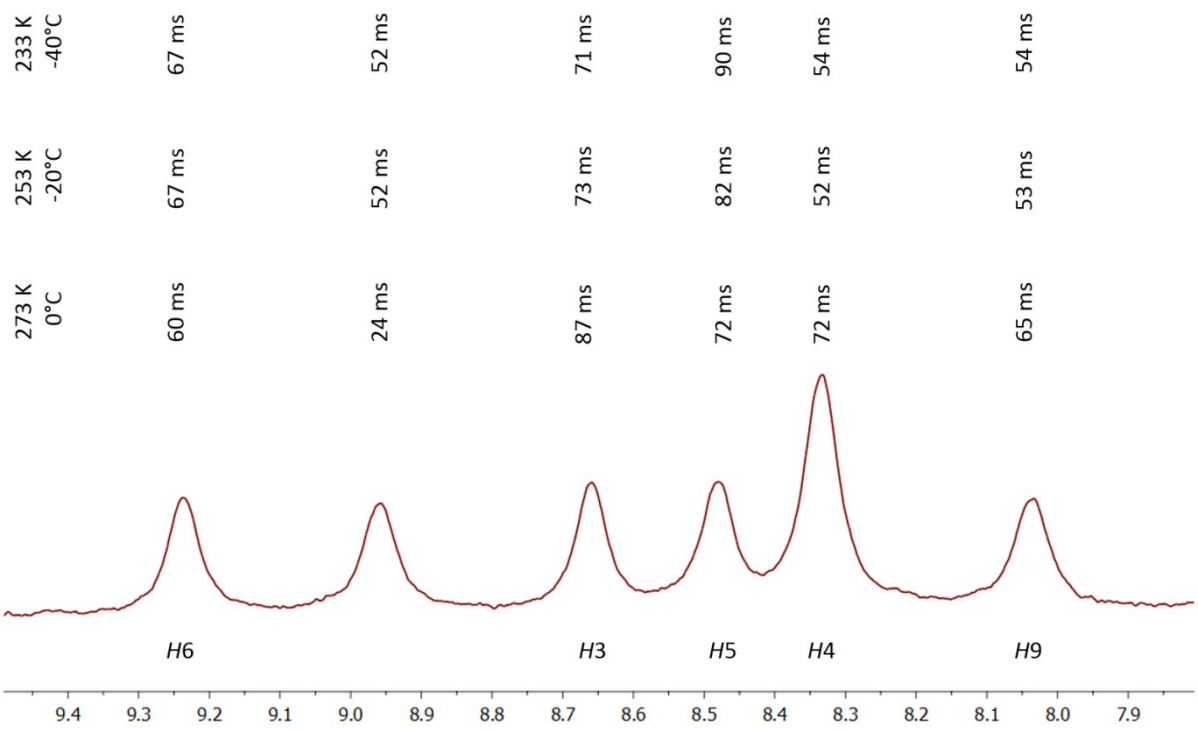

Figure 22-SI Section of ^{1}H NMR spectra of the Co^{3+} complex $[Co^{3+}(\mathbf{1})_2]^{3+}$along with the T_1 time recorded by inversion recovery experiments using a selective inversion on the Co^{3+} resonances.

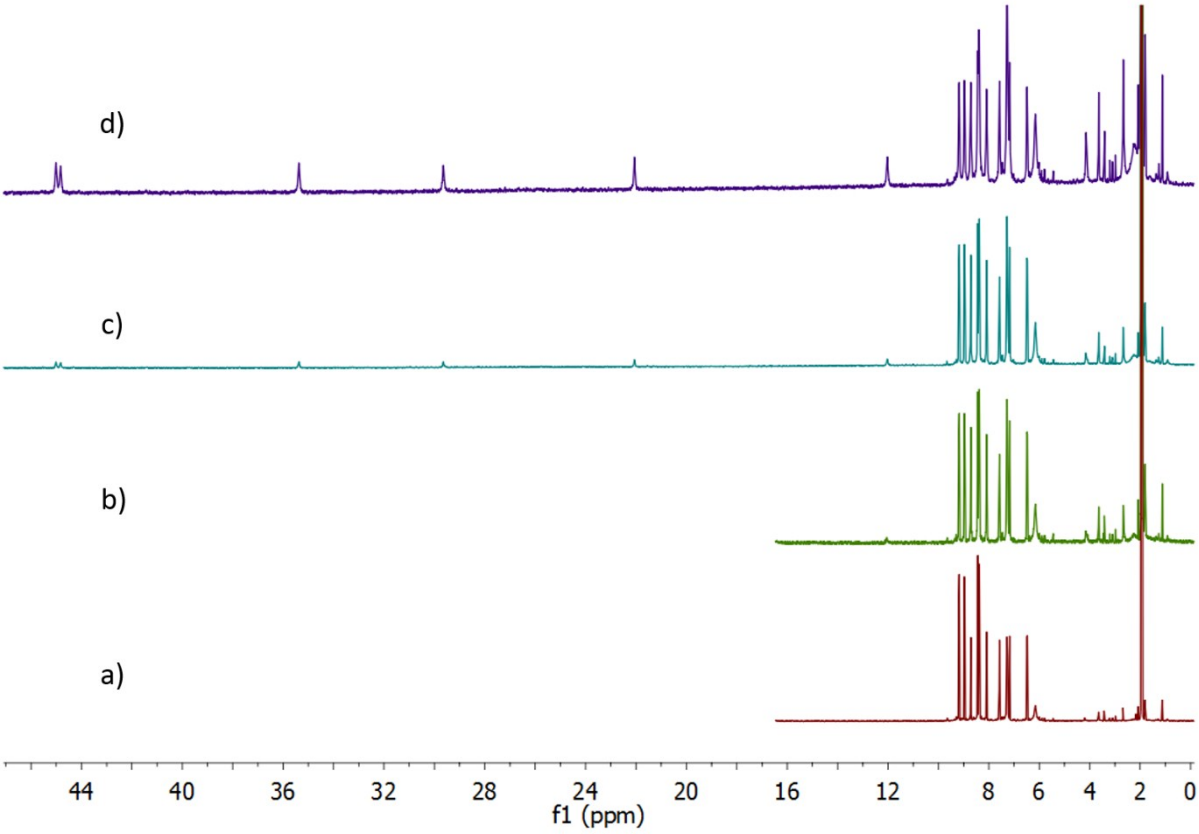

Figure 23-SI Sections of ^{1}H NMR spectra of [Co(**2**)$_2$](BF$_4$)$_3$ (a) [Co(**2**)$_2$](BF$_4$)$_3$ was reduced step-wisely with a substochimetric amount of 4-methoxy-*N,N*-di-*p*-tolylaniline (b, c, d) to generate the Co^{2+} species of the complex. The signals for the protons of the Co^{3+} species broaden due to electron transfer reactions between the cobalt cores.

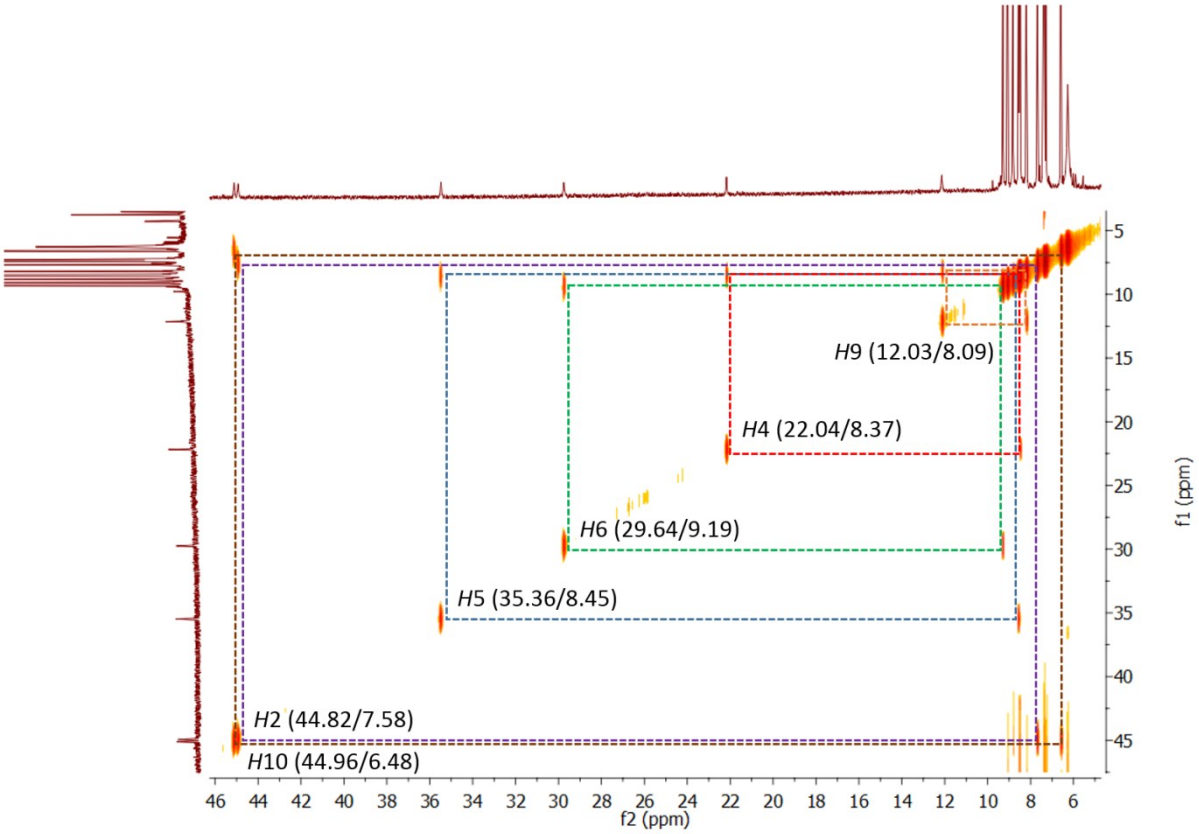

Figure 24-SI Section of $^{1}H,^{1}H$-EXSY-NMR spectrum of $[Co(\mathbf{2})_2](BF_4)_3$ which is partly reduced to $[Co(\mathbf{2})_2](BF_4)_2$ by adding a substoichiometric amount of 4-methoxy-*N,N*-di-*p*-tolylaniline. The triaryl amine is a catalyst for the electron transfer between the two cobalt species, that accelerates the electron transfer from the seconds timescale to the ms timescale. The values given in brackets are the chemical shifts in ppm for the Co^{II} and Co^{III} species respectively.

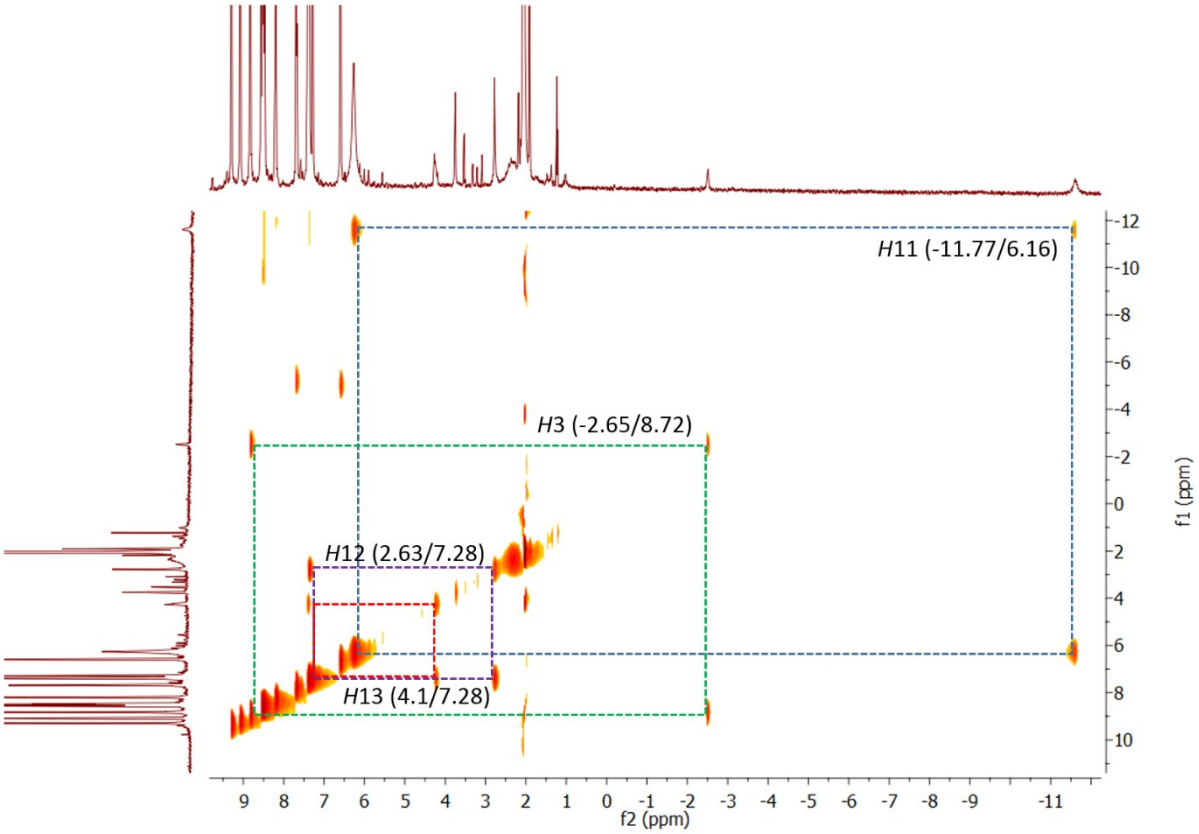

Figure 25-SI Section of $^{1}H,^{1}H$-EXSY-NMR spectrum of $[Co(\mathbf{2})_2](BF_4)_3$ partly reduced to $[Co(\mathbf{2})_2](BF_4)_2$ by adding a substoichiometric amount of 4-methoxy-*N,N*-di-*p*-tolylaniline. The triarylamine is a catalyst for the electron transfer between the two Cobalt species, that accelerates the electron transfer from the seconds timescale to the ms timescale. The values given in brackets are the chemical shifts in ppm for the Co^{2+} and Co^{3+} species respectively.

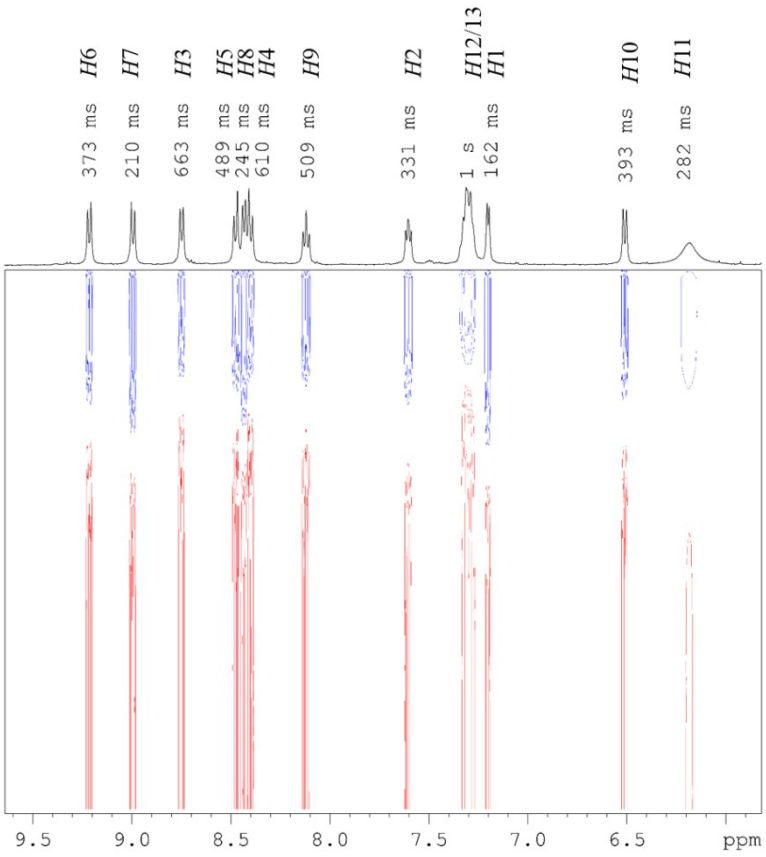

Figure 26-SI Inversion recovery experiment to determine the T_1 measurement of $[Co(\mathbf{2})_2](BF_4)_3$. The plot shows the inverted signals (red) at the bottom and recovering of the z-magnetisation with increased delay (from bottom to top). The T_1 times are typical short for diamagnetic LS-Co^{3+} complexes due to the exchange with paramagnetic Co^{2+} complex accelerated by the redox catalyst.

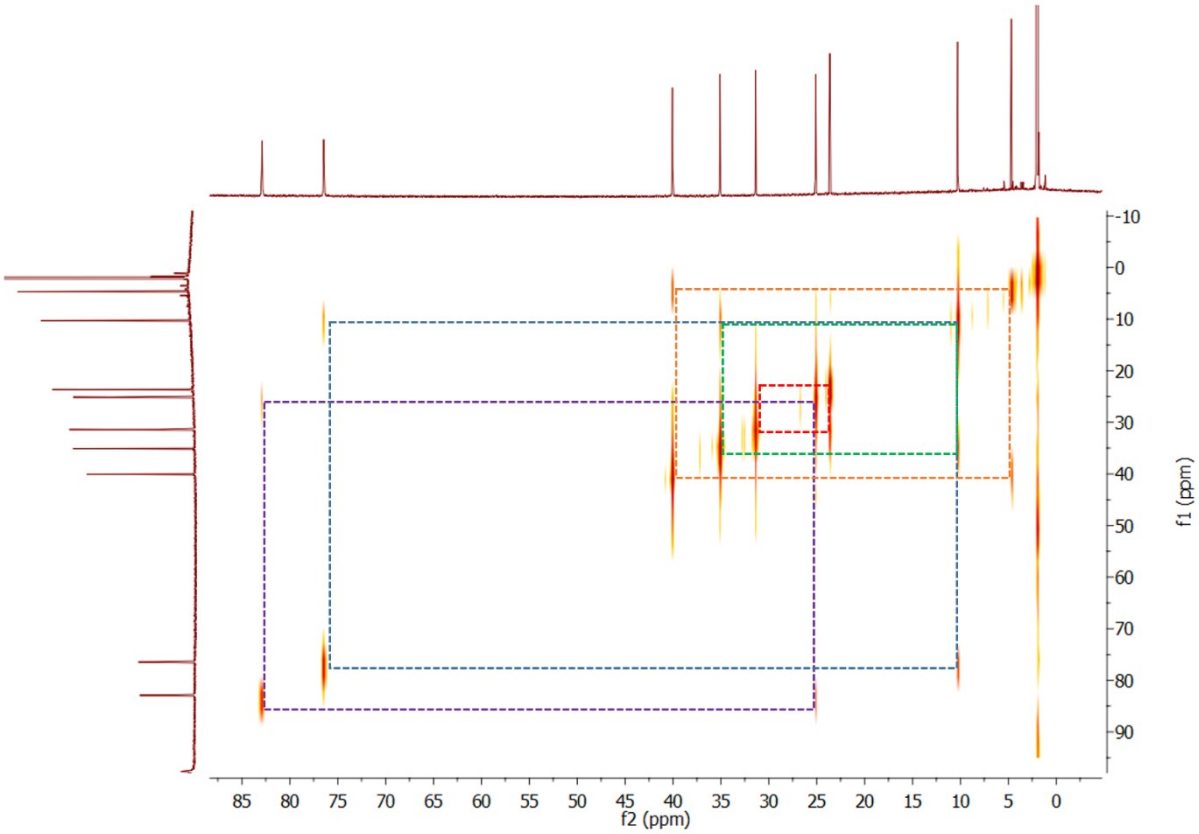

Figure 27-SI ^{1}H,^{1}H-COSY spectra of [Co(**3**)$_2$](ClO$_4$)$_2$ in d_3-MeCN at 25°C.

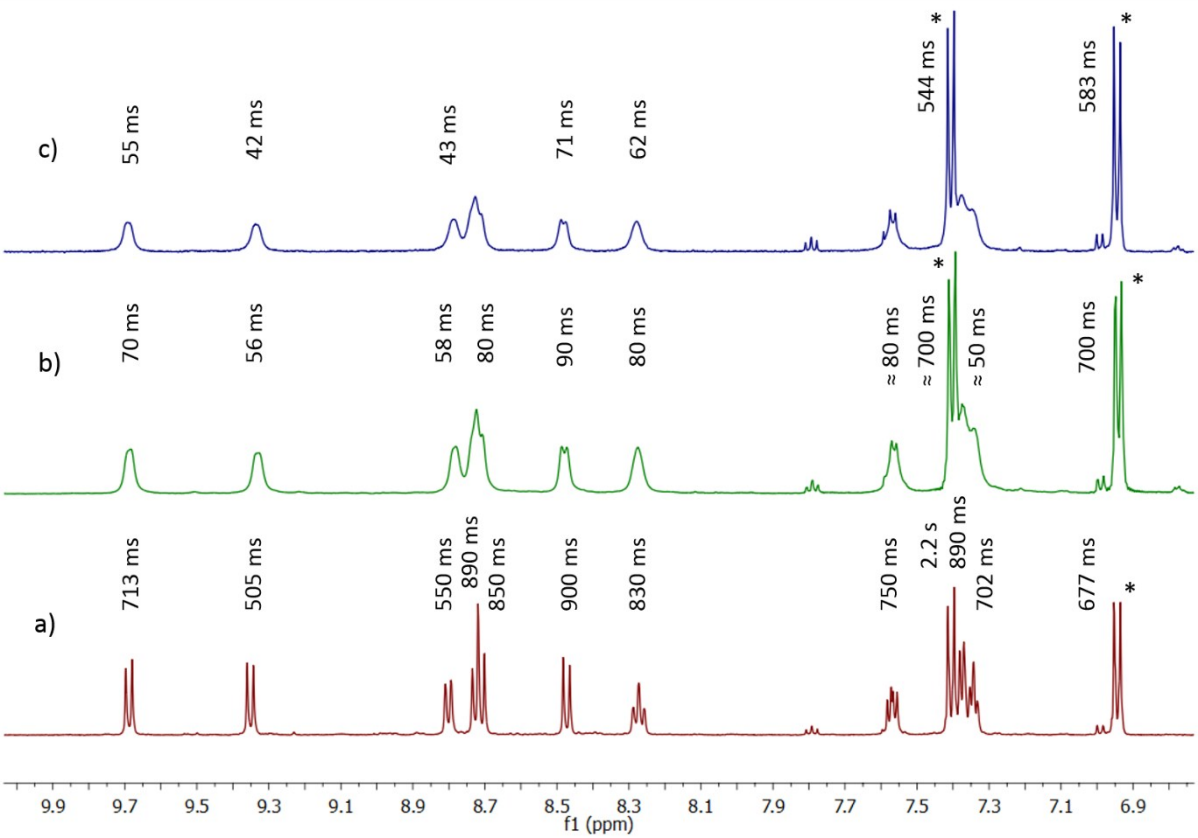

Figure 28-SI ^{1}H NMR spectra of *in situ* obtained $[Co(\mathbf{3})_2](ClO_4)_3$ (a) with T_1 values. After acetylferrocene is added (1 eq in b, 2 eq in c) the signals broaden. The signals at 7.41 and 6.94 ppm (*) are assigned to the protons of the oxidant (N-(*p*-$C_6H_4Br)_3)(SbCl_6)$. The T_1 times are atypical short for diamagnetic LS-Co^{3+} complexes due to the exchange with the paramagnetic Co^{2+} complex accelerated by the redox catalyst.

1.8.2 Oxidation attempts monitored with ^{1}H NMR spectroscopy

The oxidation of the complexes was achieved by mixing the appropriate complex with “magic blue” (Sigma-Aldrich) (**Figure *29-SI***) in d_3-MeCN in a NMR tube.

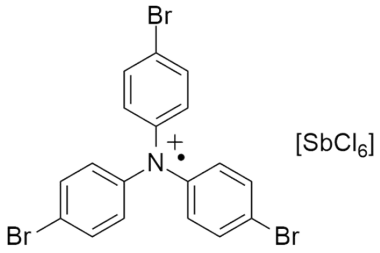

Figure 29-SI "Magic blue", a triaryl amine radical cation used for oxidation of complexes $[Co(\mathbf{1})_2](ClO_4)_2$, $[Zn(\mathbf{1})_2](ClO_4)_2$ and $[Fe(\mathbf{1})_2](ClO_4)_2$

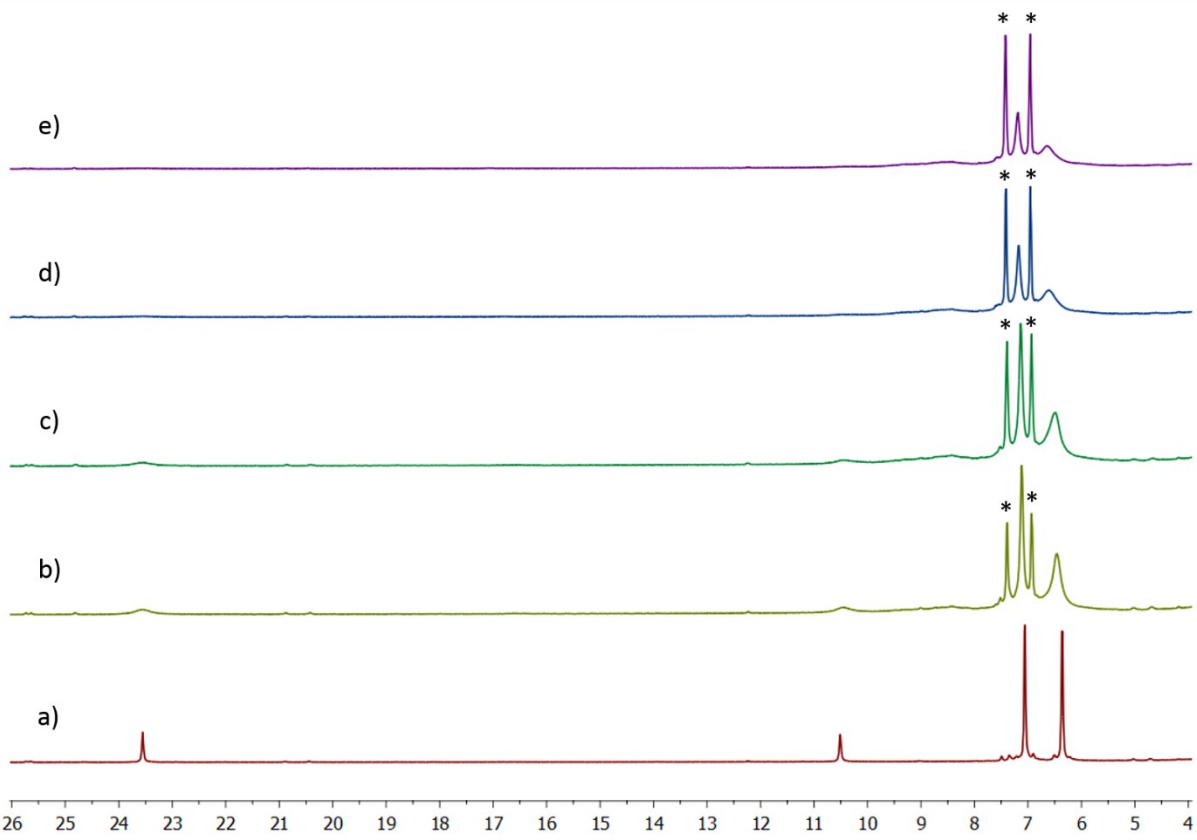

Figure 30-SI Section of ^{1}H NMR-spectra of $[Co(\mathbf{1})_2](ClO_4)_2$ in d_3-MeCN at 25°C (a). The complex was oxidised step-wisely with 0.2 eq (b), 0.35 eq (c), 0.5 eq (d) and 0.7 eq (e) of $(N(p\text{-}C_6H_4Br)_3)(SbCl_6)$. Due to impurities in the magic blue the real oxidation equivalents are lower than given under a-e. In the starting compound the signal at δ = 23.63 and 10.59 ppm are sharp and begin to broaden when the solution is mixed with the oxidant (b,c) before they disappear (d,e). The signals of the starting compound at δ = 7.14 and 6.44 ppm (Tara protons *H*13 and *H*14) are sharp and broaden in b-e as well, but not in the same extent as the other two signals mentioned before. If a substantial Tara centred oxidation would take place this should instantaneously erase this Tara-signals due to the dramatic increase of the transversal relaxation. In conclusion the first oxidation is cobalt centred. Two new signals appear for the reduced oxidant (*) $N(p\text{-}C_6H_4Br)_3$.

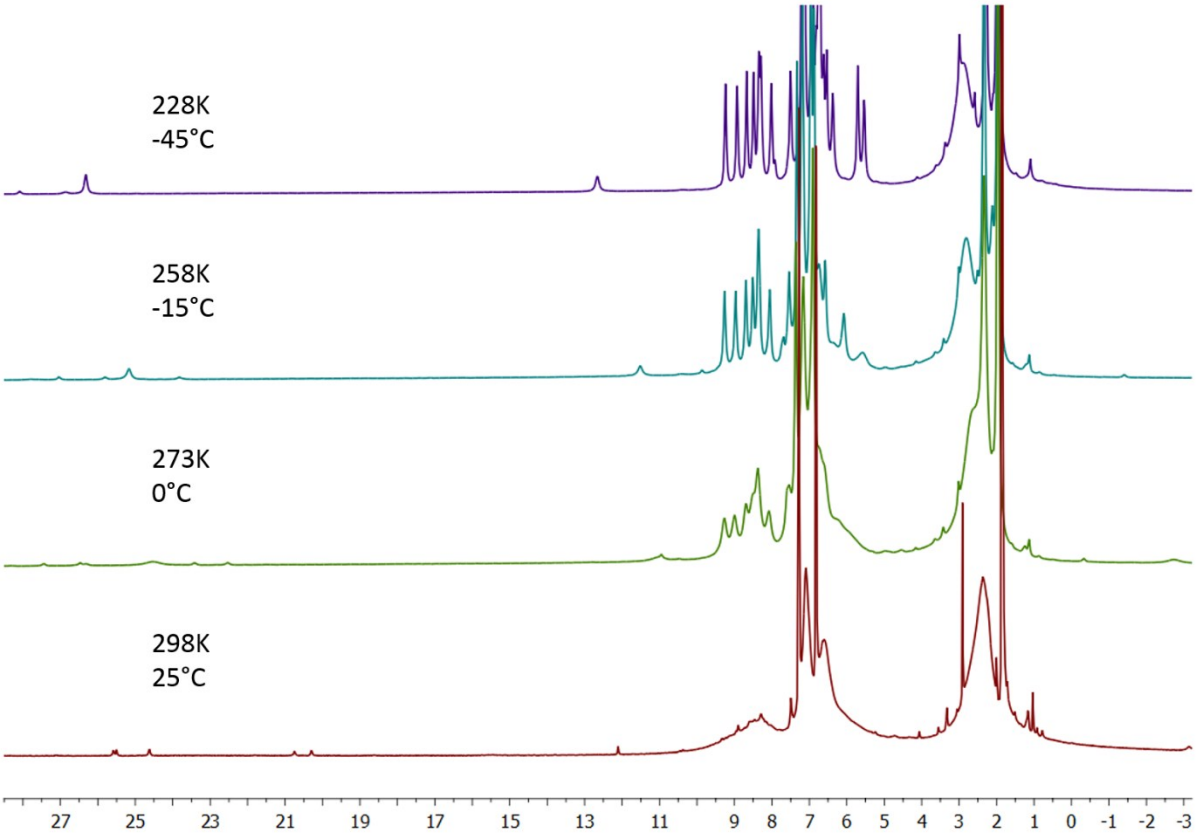

Figure 31-SI Sections of ^{1}H NMR spectra of $[Co(\mathbf{1})_2](ClO_4)_2$ in d_3-MeCN with 2 eq oxidant $(N(p\text{-}C_6H_4Br)_3)(SbCl_6)$ at 25°C (a), 0°C (b), -15°C (c) and -45°C (d). At 25°C broad signals are visible for both Co^{2+} and Co^{3+} species. At lower temperatures the signals sharpen for both redox states indicating a slower self-exchange between $[Co^{2+/3+}(\mathbf{1})_2]^{2+/3+}$.

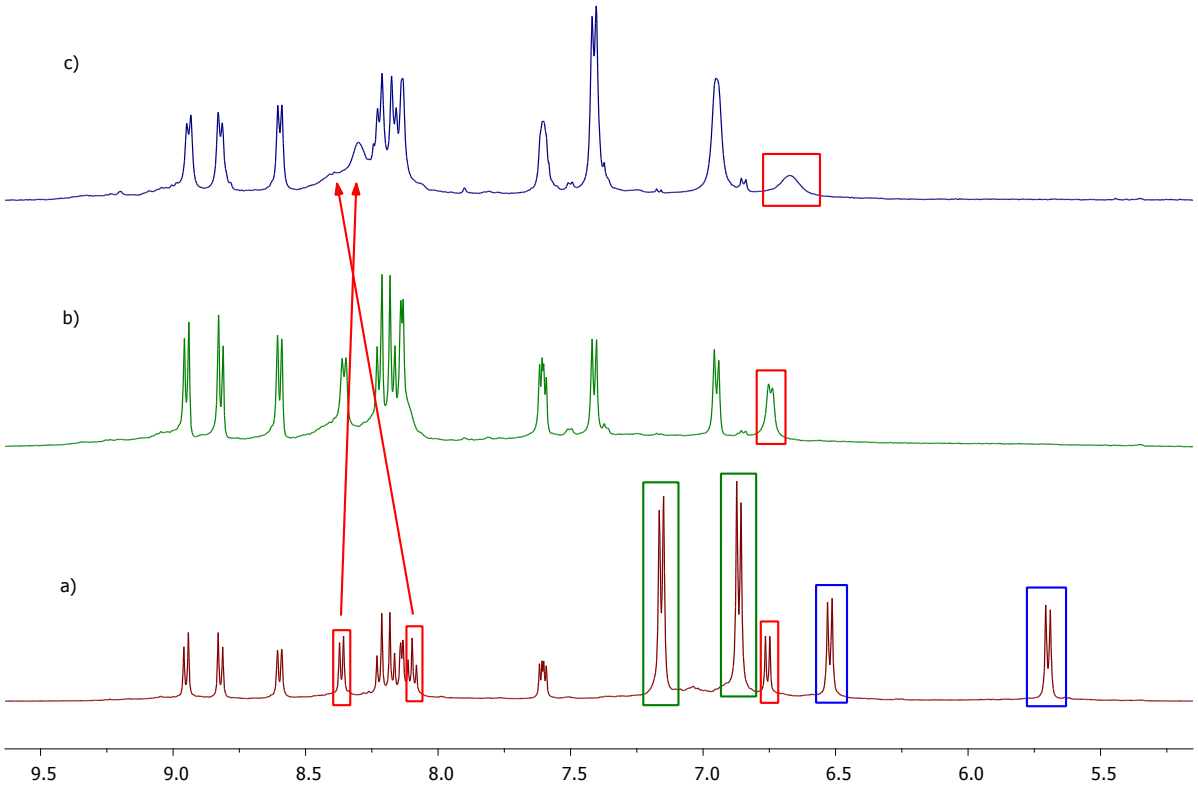

Figure 32-SI Section of ^{1}H NMR spectra of $[Zn(\mathbf{1})_2](ClO_4)_2$ in d_3-MeCN at 25°C (a). The complex was oxidised step-wisely with 0.3 eq (b) and 0.6 eq (c) of $(N(p\text{-}C_6H_4Br)_3)(SbCl_6)$. The two signal of the phenoxyl unit at δ = 6.52 and 5.70 ppm (*H*11 and *H*12, blue boxes) and the signals of the tolyl part at δ = 7.16 and 6.86 ppm (*H*13 and *H*14, green boxes) disappear completely after adding the oxidant due to the strong scalar coupling to the organic radical. Scalar coupling to an organic radical dramatically increase the transvers relaxation. The signals of the pyridine unit (red boxes) broaden after adding the oxidant which shows a small coupling of the pyridine protons with the oxidised Tara whereas the protons of the phenanthroline unit barely show any coupling or increased line broadening.

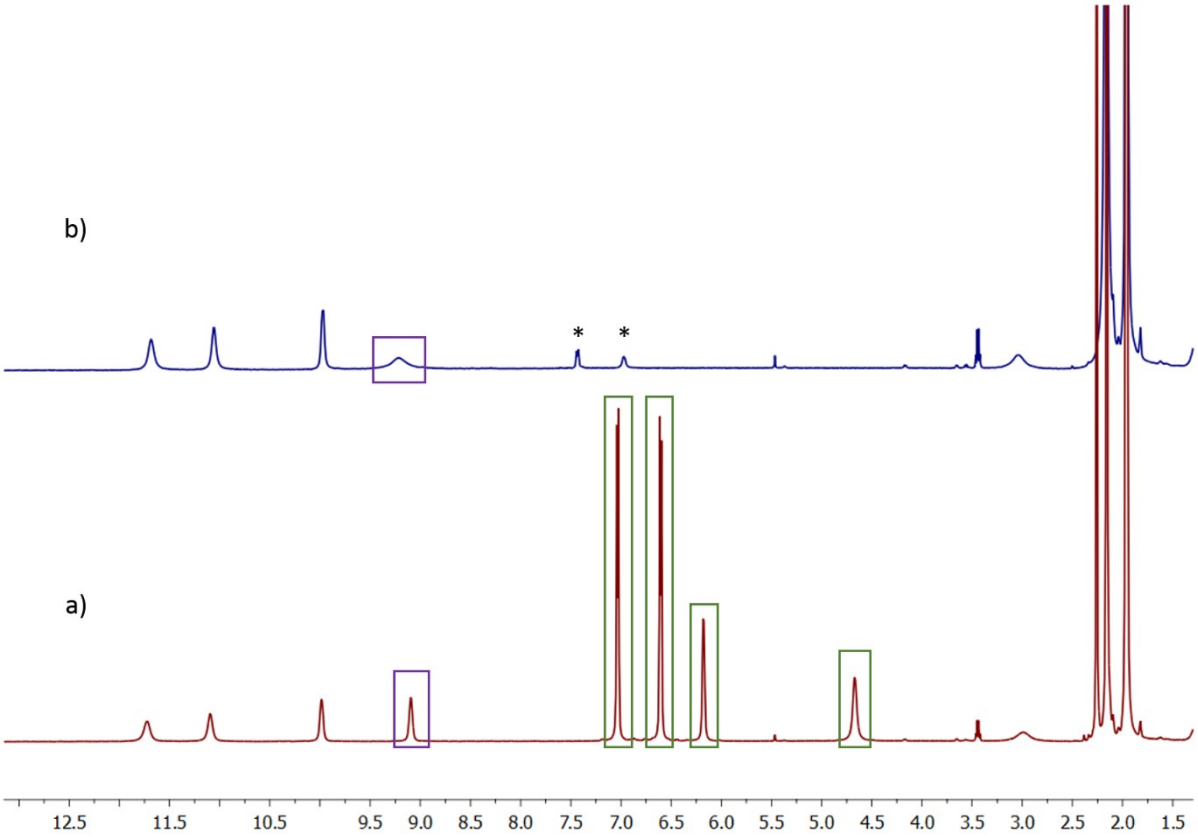

Figure 33-SI Sections of the ^{1}H NMR spectra of [Fe(**1**)$_2$](ClO$_4$)$_2$ (a) and after the addition of the oxidant (N(*p*-C$_6$H$_4$Br)$_3$)(SbCl$_6$) (b) in d_3-MeCN at 25°C. With adding the oxidant the nitrogen of the triaryl amine moiety is oxidised forming a radical cation. All the signals of the tolyl (*H*13 – *H*14), phenoxyl (*H*11 and *H*12) (green boxes) and the methyl protons disappear. Two new signals appear for the reduced (N(*p*-C$_6$H$_4$Br)$_3$)(SbCl$_6$) (*). The signal at δ = 9.10 ppm broadens after oxidation indicating a lower coupling to the Tara^{+} radical (violet boxes) than the previously mentioned protons and is assigned to a proton of the pyridyl unit. The protons of the phenanthroline unit exhibit no coupling with the triaryl amine radical cation (e.g. δ = 9.98 ppm). The results of this experiment mirror results obtained for [Zn(**1**)$_2$]$^{2+/3+}$(*vide supra*).

1.9 Estimation of the kinetics and thermodynamics of SCO on [Fe(1)$_2$]$^{2+}$

1.9.1 Thermodynamics of SCO by Vis-spectroscopy on [Fe(1)$_2$]$^{2+}$

All measurements were carried out in a homemade sample holder with a *d* = 2mm cuvette in 180° arrangement using white light LED as light source and a fiber based spectrometer Avantes ULS2048-USB2-UA-50. A detailed description of data processing is given in Ref [18]. The SCO of [Fe(**1**)$_2$]$^{2+}$ was followed by observing the absorption at 556 nm of a solution of [Fe(**1**)$_2$]$^{2+}$ in propylene carbonate. The light intensity at 638 nm served as internal reference to correct the light intensity due to sample holder expansion and shrinking. The LS state of complex [Fe(**1**)$_2$]$^{2+}$ shows typical intensive MLCT ($\varepsilon \approx$ 7000 L mol^{-1} cm^{-1}). In contrast, the HS–state can be treated as transparent below 450 nm. The absorption at 638 nm was neglected.

The light intensities were transferred in absorbance equivalent unit and the entropy and enthalpy for the SCO, $\Delta_{SCO}S$ and $\Delta_{SCO}H$ were obtained by plotting these data over 1/*T* and fitting to a sigmoidal function (**Figure *34***-SI)

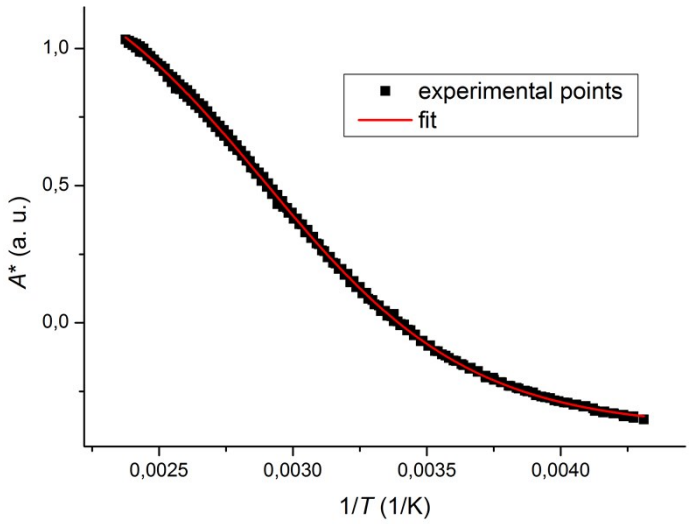

Figure 34-SI Plot and fit for the processed data of the variable temperature VT vis-experiment. From the best fit the $T_{1/2}$, $\Delta_{SCO}H$ and $\Delta_{SCO}S$ were calculated to 344(0.6) K, 21.7(0.2) kJ/mol and 63 kJ/(mol K). Errors in parentheses are statistical errors that ignore systematic errors and realistic estimates give an uncertainty of ±10 K for $T_{1/2}$ and ±5 J/(mol K) for $\Delta_{SCO}S$.

1.9.2 Estimate of SCO kinetics by ^{1}H-NMR spectroscopy on $[Fe(1)_2]^{2+}$

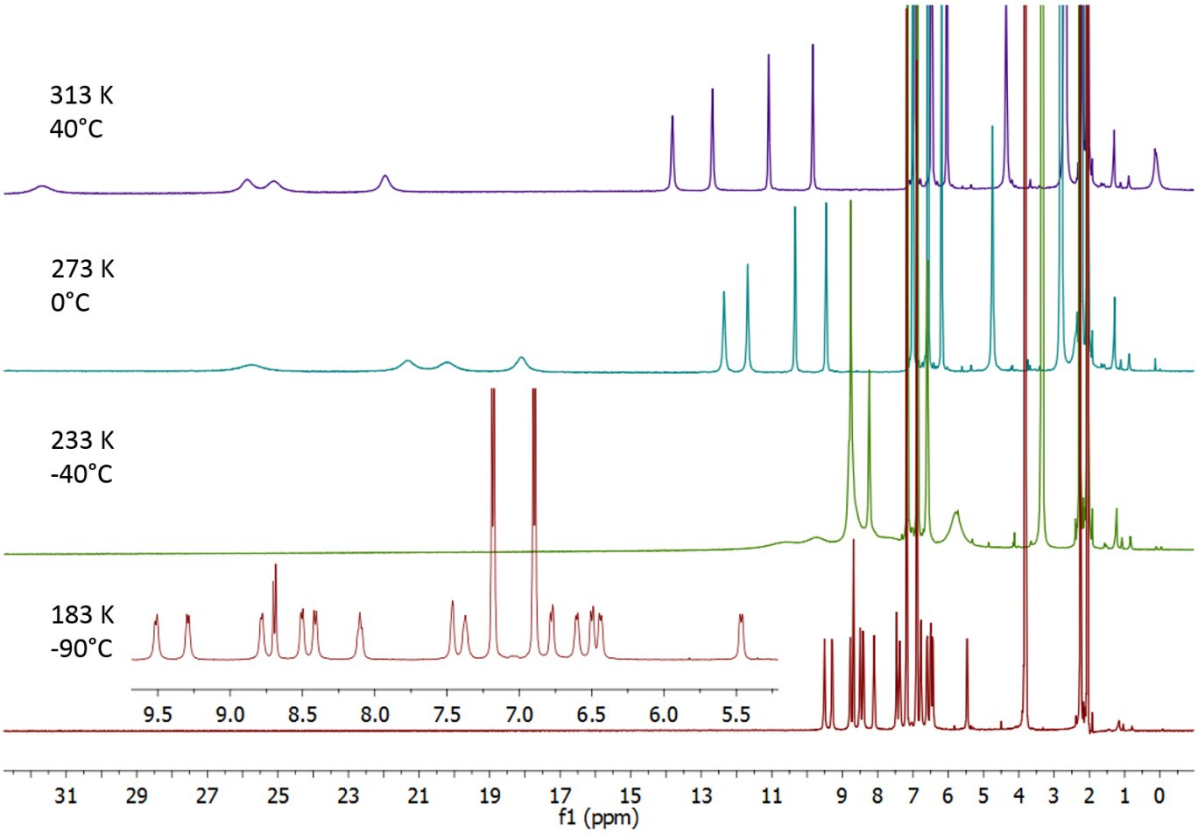

Figure 35-SI Parts of ^{1}H NMR spectra of $[Fe(\mathbf{1})_2](ClO_4)_2$ in d_6-acetone at given temperatures. Clearly visible is beginning of spin crossover 183 K. Line broadening is mainly due to exchange between the HS and LS state. A special situation is seen at 183 K, in this case the line widths of all resonances are equal and directly correspond to the LS to HS reaction rate.

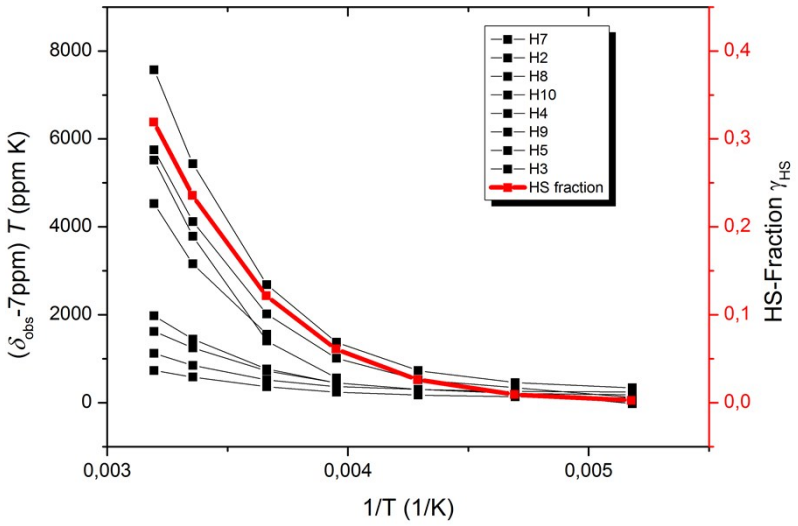

Figure 36-SI Curie Plot of the chemical shift *T* product vs. 1/*T*. Please note that for regular Curie-like behaviour a plot of the HS-fraction should be equivalent only scaled by the Curie constant. Within the errors of this experiment this is indeed the case.

Following our recently published methodology[18] the lifetimes of the HS and LS state in SCO equilibrium of $[Fe(\mathbf{1})_2]^{2+}$ were estimated using the line broadening of the NMR signals. Useful data for a rough calculation was obtained for protons *H*7 and *H*2. The chemical shift of the pure HS state, δ_{HS}, was calculated by $\delta_{HS} = (\delta_{obs} - \delta_{dia})/\gamma_{HS}$. In this equation δ_{obs} denotes the observed chemical shift. δ_{dia} denotes the diamagnetic contribution, an estimate from the chemical shift at 183 K. γ_{HS} denotes the HS fraction calculated from thermodynamic data obtained by VT-Vis spectroscopy. The contribution of the transversal relaxation to the linewidths was calculated using the longitudinal relaxation times T_1 (59 ms and 64 ms for *H*7 and *H*2 respectively at RT) that have a constant ratio to the transversal relaxation determined by the electron relaxation time and the viscosity. As shown previously the ratio for similar complexes is 1.5.[18] The linewidths for *H*7 and *H*2 were calculated to 11 Hz, the difference between calculated and observed linewidths (215 Hz and 183 Hz for *H*7 and *H*2) is attributed to the exchange broadening. The difference in Larmor frequencies between HS and LS state are $\Delta\omega = 2\pi\cdot\delta_{HS}$. Using equation (1b), derived from (1) and (1a), k_{ex} can be calculated. k_{ex} is the sum of the forward and backward reaction. By using γ_{HS} the time constants for the transformation of the LS state to HS state were calculated to 313 ns and 411 ns and for the reverse process to 96 and 126 ns. This is only a rough estimate with drastically simplification, for further discussion of the EPR spectra we assume a time constant of 250 to 450 ns for the transformation of the LS state to the HS state.

$$\frac{1}{T_{2(obs)}} = \left\{(1-\gamma_{HS})\frac{1}{T_{2(LS)}} + \gamma_{HS}\frac{1}{T_{2(HS)}}\right\} + \left\{\gamma_{HS}(1-\gamma_{HS})\frac{\Delta\omega^2}{k_{ex}}\right\} \qquad (1)$$

$$\frac{1}{\pi\cdot LW} = \left\{\frac{1}{1.5\cdot T_1}\right\} + \left\{\gamma_{HS}(1-\gamma_{HS})\frac{\Delta\omega^2}{k_{ex}}\right\} \qquad (1a)$$

$$\frac{\left\{\frac{1}{\pi \cdot LW}\right\} - \left\{\frac{1}{1.5 \cdot T_1}\right\}}{\gamma_{HS}(1-\gamma_{HS})(\Delta\omega^2)} = \left\{\frac{1}{k_{ex}}\right\} \qquad (1b)$$

The correlation time of the electron relaxation for the Tara radical $[Fe(\mathbf{1}^{+})_2]^{4+}$ can be estimated by using the linewidths of EPR spectrum, in this case roughly 0.5 G. This can be transferred into a correlation time of τ_{S2} = 210 ns at ambient temperature.

References-SI

(1) Moore, J. J.; Nash, J. J.; Fanwick, P. E.; McMillin, D. R.; *Inorg. Chem.* **2002**, *41* (24), 6387.

(2) Quinton, C.; Alain-Rizzo, V.; Dumas-Verdes, C.; Clavier, G.; Miomandre, F.; Audebert, P.; *Eur. J. Org. Chem.* **2012**, *2012* (7), 1394.

(3) Zong, R.; Wang, D.; Hammitt, R.; Thummel, R. P.; *J. Org. Chem.* **2006**, *71* (1), 167.

(4) Sheldrick, G. M.; *Acta Crystallogr. Sect. A Found. Crystallogr.* **1990**, *46* (6), 467.

(5) Sheldrick, G. M. *SHELXL-97, Program for Crystal Structure Refinement, University of Göttingen*; 1997.

(6) Sheldrick, G. M.; *Acta Cryst.* **2008**, *A24*, 112.

(7) Farrugia, l. J.; *J. Appl. Cryst.* **2012**, *2012* (45), 849.

(8) Spek, A. L.; *Acta Crystallogr., Sect. C Cryst. Struct. Commun.* **2015**, *C71*, 9.

(9) Spek, A. L.; *J. Appl. Cryst.* **2003**, *36*, 7.

(10) Spek, A. L.; *Acta Crystallogr., Sect. D* **2009**, *65*, 148.

(11) Neudeck, A.; Petr, A.; Dunsch, L.; *Synth. Met.* **1999**, *107* (3), 143.

(12) Barrière, F.; Camire, N.; Geiger, W. E.; Mueller-Westerhoff, U. T.; Sanders, R.; *J. Am. Chem. Soc.* **2002**, *124* (25), 7262.

(13) Barrière, F.; Geiger, W. E.; *J. Am. Chem. Soc.* **2006**, *128* (12), 3980.

(14) Amthor, S.; Noller, B.; Lambert, C.; *Chem. Phys.* **2005**, *316* (1–3), 141.

(15) Chow, H. S.; Constable, E. C.; Housecroft, C. E.; Kulicke, K. J.; Tao, Y.; *Dalton Trans.* **2005**, No. 2, 236.

(16) Connelly, N. G.; Geiger, W. E.; *Chem. Rev.* **1996**, *96*, 877.

(17) Yang, E. S.; Chan, M.-S.; Wahl, A. C.; *J. Phys. Chem.* **1975**, *79*, 2049.

(18) Petzold, H.; Djomgoue, P.; Hörner, G.; Speck, J. M.; Rüffer, T.; Schaarschmidt, D.; *Dalton Trans.* **2016**, *45* (35), 13798.